DOA CONVERGENCE OF UNSTRUCTURED DISTRIBUTED ARRAYS

WITH TIME-VARYING AND SPACE-VARYING MORPHOLOGIES

A Thesis

by

ZHONG CHEN

Submitted to the Office of Graduate and Professional Studies of
Texas A&M University
in partial fulfillment of the requirements for the degree of

MASTER OF SCIENCE

Chair of Committee,	Gregory H. Huff
Committee Members,	Robert D. Nevels
	Steven Wright
	John Valasek
Head of Department,	Miroslav Begovic

August 2017

Major Subject: Electrical Engineering

ABSTRACT

This thesis mainly focuses on the research of the factors that influence the accuracy and efficiency of a UAV-based radio frequency (RF) and microwave data collection system. Swarming UAVs can be utilized to create the unstructured morphing antenna arrays that reduce aliasing and improve convergence in sub-space direction of arrival techniques.

This thesis first reports on the ramifications of using unstructured antenna arrays based on sub-space techniques. This work evaluates the classical MUSIC algorithm and root-MUSIC algorithm, and Fourier domain root-MUSIC algorithm (FD Root-MUSIC). Compared to the MUSIC algorithm, the root-MUSIC algorithm avoids the search of spatial spectrum, reduces the computational complexity and improves the ability of real world applications.

Then, this thesis comes up with the data model for the UAV swarming system. Based on the data model, this work examines the impact of UAV swarm density and heterogeneity on synthetic aperture DOA convergence. The synthetic aperture is derived from the displacement of distributed UAVs operating in a sparse volumetric swarm. Heterogeneity arises from the changing orientation of a UAV's antenna and receiving pattern function as it swarms in the distributed cluster of UAVs. This alters the UAVs' antenna pattern functions over time and alters the convergence and overall performance properties of vector-space direction of arrival techniques. This work evaluates the impact of the swarm density and orientation in this framework and studies the convergence and

error using MUSIC algorithm. This work also discusses the impact of different type of errors introduced from UAV swarming.

Furthermore, this thesis examines the DOA convergence performance of location-varying volumetric random array using MUSIC algorithm. Simulation and measurements for up to sixteen elements on a thirty-two-location test platform are provided and comparisons are made to benchmark their performance with theoretical expectations. MATLAB simulation indicates that the volumetric random arrays can be applied in a very noisy condition by increasing the iterations and multiplying the MUSIC spectrum and experimental observations demonstrate that the system accurately capture the azimuthal and elevation angles of the source.

At last, this thesis investigates and designs the tunable FM band monopole and loop antennas to locate the FM broadcasting stations. The wavelength of the FM band is around three meters. This work uses lumped elements and meandering antenna structure technologies to reduce the antenna size and match the antenna. This work also uses the varactor diodes to tune the antenna. However, the antenna becomes electrically small and the antenna gain is so low that it cannot detect the FM signal from the local FM broadcasting stations.

ACKNOWLEDGEMENTS

I would like to thank my committee chair, Dr. Huff for his advice, guidance and full support throughout this thesis work, which has been crucial to the success of the work. It is my honor to work with him. I would also like to express my gratitude to my committee members, Dr. Nevels, Dr. Wright, and Dr. Valasek, for their unlimited time, advising and support throughout the course of this research.

I also would like to express my thanks to my colleagues in the Electromagnetic and Microwave Laboratory (EML) for their assistance and friendship during my master period.

Finally, I would like to thank my dear parents and girlfriend for their understanding, support and encouragement in my studies.

CONTRIBUTORS AND FUNDING SOURCES

This work was supervised by a thesis committee consisting of Dr. Huff, Dr. Nevels and Dr. Wright of the Department of Electrical and Computer Engineering and Dr. Valasek of the Department of Aerospace Engineering.

All work conducted for the thesis was completed by the student, under the advisement of Dr. Huff of the Department of Electrical and Computer Engineering.

There are no outside funding contributions to acknowledge related to the research and compilation of this document.

NOMENCLATURE

1D	1-dimension
2D	2-dimension
3D	3-dimension
AR	Autoregressive
ARMA	Auto-Regressive and Moving Average
DOA	Direction of Arrival
ESPRIT	Estimation Signal Parameters via Rotational Invariance Technique
FD	Fourier Domain
FDWLS	Fourier Domain Weighted Least-Squares
FM	Frequency Modulation
GPS	Global Positioning System
HFSS	High Frequency Structural Simulator
MA	Moving Average
ME	Maximum Entropy
ML	Maximum Likelihood
MS	Manifold Separation
MUSIC	Multiple Signal Classification
RF	Radio Frequency
SNR	Signal to Noise Ratio
UAV	Unmanned Aerial Vehicle
ULA	Uniform Array

NUA	Nonuniform Array
VNA	Vector Network Analyzer
VSWR	Voltage Standing Wave Ratio

TABLE OF CONTENTS

Page

LIST OF FIGURES

Page

LIST OF TABLES

1. INTRODUCTION

With the development of modern electrical and information technologies and the increasing number of applications of mobile communication technologies on various domains, a variety of information services based on advanced communication technologies have attracted more and more attentions recently, including precise positioning services like global positioning system (GPS). However, wireless positioning and direction-finding technologies are also very prevailing in civil and military applications on wireless and mobile communication, such as directing and connecting the base station using the smart antenna technology, finding the source location in the seismic exploration, positioning the interference source in the military communications, etc. Those technologies always require real-time processing, highly precise measurement, and powerful antijamming capability. Classical radar direction-finding and GPS positioning systems are not able to be suitable for those applications. Therefore, the direction of arrival (DOA) estimation technologies are developing fast.

1.1 Research Background

At present, the research on direction-finding system is mainly in two aspects: one is to research the antenna array structure; the other is to research the direction-finding algorithm.

For the research on the antenna array structure, the economic benefit of the system is very important. After satisfying the system performance, it always optimizes the array structure by reducing the number of the elements, which not only keeps the system simple,

but also reduces the cost by decreasing the complexity of the system. Since the application conditions are very complex in the military, the antenna structure is always irregular. Therefore, it is very important to optimize the irregular array structures.

For the research on the algorithm, most of the algorithms are suitable for the applications of uniform linear arrays (ULAs) under all kinds of special conditions. However, many of the algorithms are not suitable for the arbitrary planar arrays. Even though a variety of algorithms have been proposed to provide the estimation for DOA, the multiple signal classification (MUSIC) algorithm remains quite prevalent since it offers a very robust eigen-based decomposition of the signal space [4]. However, relative to the one-dimension (azimuth angle) direction-finding, the two-dimension (both azimuth and elevation angles) direction-finding causes the computational complexity considerable. Therefore, it is important to reduce the calculation of the algorithm to achieve the real-time measurement.

In sum, it is necessary to optimize the antenna array structure and research the DOA algorithm for the practical direction-finding applications.

1.2 Overview of the Development of DOA Estimation Methods

DOA estimation has been a topic of discussion for many years [1-3]. Initially, the DOA estimation based on sensor array structures used the Barlett beamformer method, which mainly contained the periodogram method and Blackman Tukey method. But, it was impacted by the Rayleigh limit so that it cannot obtain a high-resolution performance. In 1967, Burg came up with the maximum entropy (ME) method, which includes the ME, Autoregressive (AR) model, Moving Average (MA) model, Auto-Regressive and Moving

Average (ARMA) model parameter method. These methods have a high-resolution, however, they also have a low robustness and a considerable computation [5,6,7].

When it came to the 1980s, a series of high-resolution spatial spectrum estimation methods based on decomposition of matrix eigen values for array signal processing came out and created a new era. All those estimations were represented by MUSIC and estimation signal parameters via rotational invariance technique (ESPRIT) [1,8,9,10]. MUSIC algorithm had attracted more and more attentions since it came out, which was the milestone of spatial spectrum estimation. MUSIC algorithm decomposes the eigen value data from sensor arrays and divides the linear space into the orthogonal noise subspace and signal subspace. Then, it builds up the space spectrum using the orthogonal property. In certain conditions, the MUSIC algorithm is one-dimensional implementation of maximum likelihood (ML) method, which share the same character with ML [11,12]. However, it has the weakness of heavy calculation, large buffer memory and high dependence on the signal model. In 1983, some search-free algorithms, such as root-MUSIC, use root-solving technique to reduce the computational complexity [13,14]. The similar case is that ESPRIT algorithm and its improved algorithms such as LS-ESPRTI, TLS-ESPRIT and MI-ESPRIT avoid large computation in spectrum-searching, so it can increase the speed of DOA estimation. However, it can only be used under the special array structure to achieve the DOA estimation, so the practical application is relatively narrow [15].

Recently, some researchers proposed that the classical DOA estimation algorithms, such as ML, MUSIC and ESPRIT, did not include the time characteristic of the signal. It

is necessary to add the appropriate time-domain data processing into the process of spatial-domain data processing by using sufficiently the useful information of the signals. Researchers think we can sample the signals in the time domain and spatial domain at the same time. The 2D array signal processing method improves the ability of resistance to noise and reduces the restraint of array structure.

Furthermore, recently researchers would like to employ the array signal processing method based on higher-order cumulant to reduce the colored noise in the environment, due to the natural blind feature for any Gaussian noise of the higher-order cumulant [16]. The algorithm can expand the classical DOA estimation algorithms to Gaussian spatial colored noise or symmetric distributed non-Gaussian spatial white noise and colored noise by using the cumulative amount. It also can enlarge the array aperture to some extent.

Most of these methods are still in the experiment, simulation and theoretical stage, which is far from actual applications. The Massachusetts Institute of Technology (MIT)'s Lincoln Laboratory proposed that, MUSIC algorithm based on spatial spectrum was a leading candidate and the most promising for further study and actual hardware implementation among currently accepted super-resolution algorithms, after a detailed evaluation of thousands of simulations [17]. People usually choose the MUSIC algorithm to do research in the actual applications.

1.3 Summarized Contributions Made by This Thesis

The first contribution of this thesis is to apply FD Root-MUSIC onto volumetric antenna arrays to estimate both the azimuthal and elevational angles firstly. The classical MUSIC algorithm needs a lot of computational quantity due to spectrum-searching, the

FD Root-MUSIC algorithm solves the roots of the spectrum polynomial to obtain the incident signal angles estimation. The peaks in the spectrum space correspond to the roots of the polynomial lying close to the unit circle. However, when the number of the array elements is very big, the computational complexity is super high, so it is important to process the data reasonably.

The second contribution of this thesis is to create the UAV swarm model when the array is swarming. This model includes the gain and phase pattern effects, and environment noise when the array swarms with time. Bases on the model, this work investigates the DOA performance of unstructured distributed arrays with space-varying and time-varying morphologies. The UAV swarm morphs over time to create a synthetic aperture, which alters the position and orientation of agents in the swarm. This work evaluates the impact of swarm density and heterogeneity.

The third contribution of this thesis is to investigate the impact of different type of errors including uniformly and normal distribution errors as the UAVs swarm. Since the swarming UAVs change the orientation and receiving pattern, the DOA estimation performance properties are altered. This work adds this factor to promote the DOA performance.

1.4 Thesis Organization

This thesis firstly introduces the research background and significance of DOA arrival estimation, and the overview of the DOA algorithm. MUSIC and modified MUSIC algorithms are still prevalent in the modern DOA estimation. Chapter 2 describes the ramifications from using unstructured arrays in sub-space DOA techniques. Chapter 3

presents the impact of the UAV smarm density and heterogeneity of the synthetic aperture on DOA convergence. The antenna pattern morphing as the UAV swarms is consider into the DOA convergence. Different kind of errors are introduced in the UAV swarming system. Chapter 4 examines the impact of the location varying volumetric random array on DOA convergence, which proves that it can be applied under a very noisy condition using MUSIC algorithm. In chapter 5, tunable FM band monopole and loop electrically small antennas are investigated and designed. However, the electrically small antenna's gain is too low and cannot detect the FM band signal from the local radio broadcasting stations. Chapter 6 concludes the thesis.

2. UNSTRUCTURED ARRAYS IN SUBSPACE METHODS

2.1 Classic MUSIC Algorithm

In 1986, Dr. Schmidt came up with the MUSIC algorithm [1], which was the theoretical cornerstone of the spatial spectrum estimation technology. Many algorithms proposed later in this area were under the inspiration of the MUSIC algorithm. Even though it has been studied for several decades, it is still popular in DOA estimation due to high resolution.

2.1.1 Data Model

Figure 1 shows a graphical representation of the M receiving array elements and D incident wave fronts and noise.

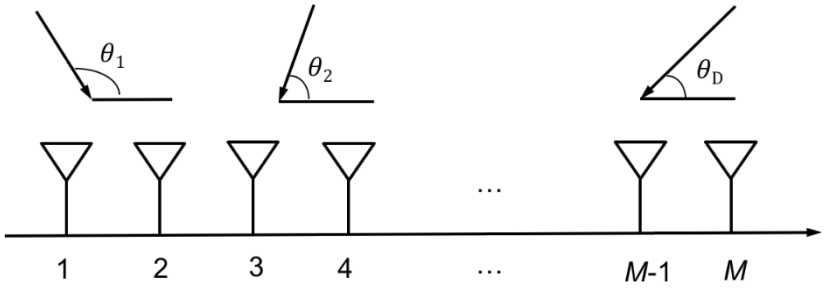

Figure 1. MUSIC algorithm model.

Assume the waveforms received at the *M* receiving array elements are linear combinations, thus a model can be created as representing the received vector signals *X* in:

$$\begin{bmatrix} X_1 \\ X_2 \\ \vdots \\ X_M \end{bmatrix} = \left[a(\theta_1) \;\; a(\theta_2) \cdots a(\theta_D) \right] \begin{bmatrix} F_1 \\ F_2 \\ \vdots \\ F_M \end{bmatrix} + \begin{bmatrix} W_1 \\ W_2 \\ \vdots \\ W_M \end{bmatrix} \tag{1}$$

or

$$X = AF + W \tag{2}$$

where, M is the number of the receiving array elements; D is the number of the incident signals; X is the M $\times 1$ received vector signals, including the phase difference and noise; A is the M $\times$ D matrix of the steering vector, determined by the signal arrival angle and the antenna array locations; F is the weighted coefficients; W is the complex vector noise.

2.1.2 Covariance Matrix R

Supposing the noise is the Gaussian white noise with zero mean and variance σ^2, and the noise and the incident signals are uncorrelated. Thus, the M $\times$ M covariance matrix R of X can be obtained here:

$$\begin{aligned} R &= E[XX^H] \\ &= E[AFF^H A^H] + E[WW^H] \\ &= APA^H + \sigma^2 I \end{aligned} \tag{3}$$

Where, $P = FF^H$ is diagonal and merely positive definite since the incident signal is uncorrelated.

2.1.3 Signal and Noise Subspaces

Define:

$$R_S = APA^H \tag{4}$$

R_S is the M × M matrix with rank D, therefore, it has the M-D repeated eigenvectors corresponding to the minimum eigenvalues (zero eigenvalues).

Let e_i be such an eigenvector, thus:

$$R_s e_i = 0 \tag{5}$$

or

$$A^H e_i = 0 \tag{6}$$

That is, the M-D eigenvectors (e_i) corresponding to zero eigenvalues are orthogonal to the D signal steering vectors.

Define,

Noise subspace: M-D dimensional subspace spanned by the noise eigenvectors.

Signal subspace: D dimensional subspace spanned by the incident signal mode vectors.

2.1.4 Algorithm

Let Q_n be the M × (M-D) matrix of the noise eigenvectors. Then, we can structure the MUSIC spatial spectrum function,

$$P_{MU}(\theta) = \frac{1}{a(\theta)^H Q_n Q_n{}^H a(\theta)} = \frac{1}{\left\| Q_n{}^H a(\theta) \right\|^2} \tag{7}$$

Then, search the spectrum peaks in the range of θ and the spectrum points we obtain are the estimation of the arrival angles of the incident waves.

2.1.5 Simple Example for MUSIC Algorithm

One simple example of DOA estimation using two elements is shown below. Assume that the DOA is 60° and the spacing is 0.5 λ.

(1) Measure the phase information from S_{21}:

$$\phi_n = \begin{bmatrix} 0.5000 \\ 2.1208 \end{bmatrix} \text{ rad}$$

(2) Calculate the phase difference:

$$\Delta\phi_n = \begin{bmatrix} 0 \\ 1.6208 \end{bmatrix} rad$$

(3) Calculate the vectors mapped on the polar coordinate:

$$X = e^{j\Delta\phi_n} = \begin{bmatrix} 1 \\ -0.05 + 0.9988 * j \end{bmatrix}$$

(4) Calculate the covariance matrix R and perform the decomposition of R:

$$R = X * X^H = \begin{bmatrix} 1 & \text{-0.05-0.9988}* j \\ \text{-0.05+0.9988}*j & 1 \end{bmatrix}$$

$$[Q,D] = eig(R)$$

$$\text{Eigen vectors: } [Q] = \begin{bmatrix} 0.7071 & 0.7071 \\ -0.0353 + 0.7062 * j & 0.0353 - 0.7062 * j \end{bmatrix}$$

$$\text{Eigen values: } [D] = \begin{bmatrix} 2 & 0 \\ 0 & 1.0447e(-33) - 5.64e(-17) * j \end{bmatrix}$$

Therefore, the noise subspace:

$$Q_n = \begin{bmatrix} 0.7071 \\ \text{0.0353-0.7062}*j \end{bmatrix}$$

and the signal subspace,

$$Q_s = \begin{bmatrix} 0.7071 \\ -0.0353 + 0.7062 * j \end{bmatrix}$$

(5) Perform the search in the searching space [0 π] rad:

$$P_{MUSIC}(\theta) = \frac{1}{a(\theta)^H Q_n Q_n^H a(\theta)} = \frac{1}{\left\| Q_n^H a(\theta) \right\|^2}$$

where $a(\theta) = e^{j\Delta\phi}$ and $\Delta\phi$ increases from 0 to π with the step 0.01 rad.

(6) Plot the MUSIC spectrum as shown in Figure 2.

(7) Obtain the estimated DOA:

The estimated DOA corresponds to the peak value in MUSIC spectrum. In this case, DOA is about 60.5 degree and close to the actual DOA. The small error is due to the noise existing in the phase difference information.

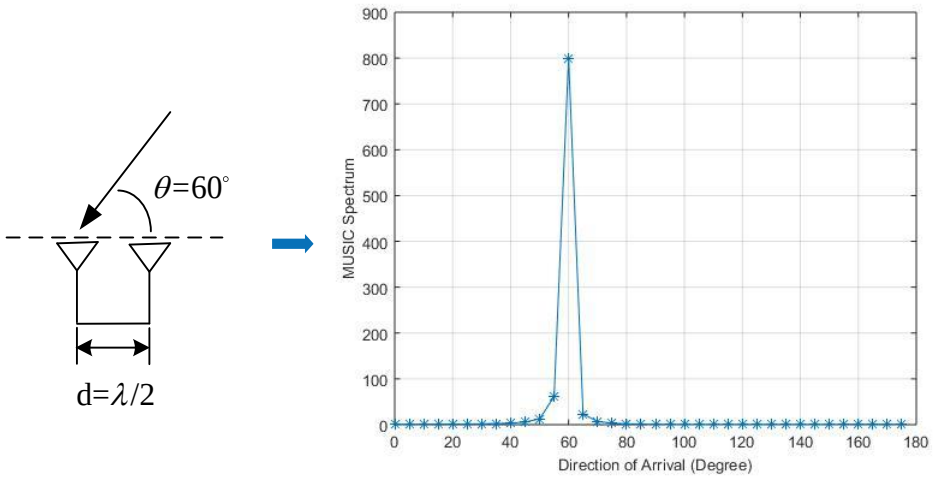

Figure 2. MUSIC spectrum.

2.2 Root-MUSIC Algorithm

The disadvantage of the MUSIC algorithm is heavy computation, whereas the root-MUSIC avoids the spectrum-searching by solving the roots of the polynomial. Thus, the root-MUSIC method can improve the code efficiency. However, the standard root-MUSIC is only suitable for uniform linear array (ULA) and nonuniform array (NUA) which lies on a uniform grid. The interest of developing search-free DOA estimation technologies for arbitrary array geometries has been increased. There are four popular search-free algorithms based on root-MUSIC algorithms: 1) The first is the interpolated root-MUSIC algorithm, which achieves the purpose by using a virtual ULA to approximate any actual NUA [18,19]; 2) The second is manifold separation (MS) algorithm based on root-MUSIC, which models the received wavefield using an orthogonal extension and a Vandermonde vector on the basis of the angle and array geometry [20,21,22]; 3) The third is the Fourier domain (FD) root-MUSIC algorithm, which finds that the null-spectrum MUSIC function is periodic in angle and uses the truncated Fourier series expansion of this periodic function to reformulate the DOA estimation problem by solving the roots of polynomial functions [10]; 4) The last is the FD-Weighted Least-Squares (FDWLS) root-MUSIC algorithm, which uses a weighted least-squares approximation of the MUSIC null-spectrum function [10].

2.2.1 Standard Root-MUSIC Algorithm

In this section, the ULA case would be introduced to demonstrate the basic knowledge of the standard root-MUSIC algorithm. The standard MUSIC algorithm has been derived from section 3.2. Since the signal subspace and noise subspace are

orthogonal, therefore, we can construct the polynomial f_z using the noise subspace Q_n for ULAs, such that

$$f_z = V^H Q_n Q_n{}^H V = 0 \tag{8}$$

where the steering vector V is

$$z = [1 \; z^{-1} \; z^{-2} \cdots z^{-(M-1)}]^T \tag{9}$$

and

$$z = e^{j\frac{2\pi d}{\lambda}\sin(\theta)} \tag{10}$$

where d is the spacing among the ULAs, the λ is the wavelength, and θ is the incident angle.

The roots of f_z contain the DOA information. Ideally, the roots should be in the unit circle at locations, however, it may not at the unit circle due to the presence of the noise. For each root, we can find the incident angle by the equation,

$$\theta_k = \arcsin[\frac{\lambda}{2\pi d}\arg(z_k)] \tag{11}$$

2.3 Fourier Domain Root-MUSIC Algorithm

2.3.1 Classical Fourier Domain Root-MUSIC Algorithm

The Fourier domain Root-MUSIC (FD Root-MUSIC) algorithm came up with first by Rubsamen and Gershman in [10] uses a different approach from root-MUSIC algorithm

to obtain a polynomial. They found that the MUSIC null-spectrum function has a period 2π in θ. Thus, Fourier series expansion can be used to rewrite the function as

$$f(\theta) = \sum_{m=-\infty}^{\infty} F_m e^{jm\theta} \tag{12}$$

where F_m are the Fourier series coefficients, which can be expressed as

$$F_m = \frac{1}{2\pi} \int_{-\pi}^{\pi} f(\theta) e^{-jm\theta} d_\theta \tag{13}$$

The function (θ) can be approximated by truncating the Fourier series in (12) to $2M_1$-1 points as

$$\begin{aligned} f(z) &\approx \sum_{m=-(M_1-1)}^{M_1-1} F_m e^{jm\theta} = \tilde{f}(\theta) \\ &= \sum_{m=-(M_1-1)}^{M_1-1} F_m z^m = \tilde{f}(z) \end{aligned} \tag{14}$$

where the $z = e^{j\theta}$, which is different from that used in (10).

The discrete Fourier transform (DFT) can be used to obtain the Fourier series coefficients F_m as

$$F_m \approx \frac{1}{2\pi} \sum_{l=-(M_1-1)}^{M_1-1} f(l\Delta\theta) e^{-jml\Delta\theta} \Delta\theta = \hat{F}_m \tag{15}$$

where $\Delta\theta = 2\pi / (2M_1 - 1)$. The final expression of the FD Root-MUSIC polynomial could be expressed by the DFT approximation as

$$\tilde{f}(z) \approx \sum_{m=-(M_1-1)}^{M_1-1} \hat{F}_m z^m \tag{16}$$

Since aliasing effects are brought in due to sampling the MUSIC null-spectrum function (θ), the DFT coefficients $\hat{F}_m$ are different from the Fourier series coefficients F_m. Increasing M_1 can reduce the aliasing effect, but this will enhance the computational complexity.

2.3.2 Apply the FD Root-MUSIC Algorithm to 2D DOA Estimation

The FD Root-MUSIC algorithm can be applied in arbitrary NUAs, but it cannot be extended simply to the 2D (azimuth and elevation angles) DOA estimation. Since the roots close to the unit circle only exist in the incident angle, so we can search the elevation angle to find the roots to calculate the azimuth angles, the corresponding elevation angles are the incident angles. Below is the process:

1) Step 1, calculate the covariance matrix

$$R_X = \frac{1}{N} \sum_{k=1}^{N} X(k) X^H(k) \tag{17}$$

where X is the receiving data matrix, and judge the number of the incident signals by AIC criterion;

2) Step 2, search the elevation angle from (0, π);

3) Step 3, for a given elevation angle θ, calculate the Fourier series coefficients F_m using the formula (15);

4) Construct the polynomial and find the roots of the polynomial and judge if there is a root close to the unit circle, if so, calculate the azimuth angle and the relative elevation

angle is the estimated angle; if not, it means there is not arrival angle in the certain elevation angle θ, go to step 5;

5) Repeat step 3 and 4 for the next elevation angle θ, obtain the estimated angles of all the signals.

2.3.3 Example for FD Root-MUSIC Algorithm

Simple ULA and NUA are introduced for 1D DOA estimation using FD root-MUSIC algorithm. Spherical array and volumetric random array are also discussed for 2D DOA estimation.

First, this work uses a ULA as an example, and the array structure is shown in Figure 3. Uniform linear array. The roots of the polynomial are the same as Figure 4. Table 1 shows that when the incident angle is 50°, the estimated angle is 130°, which is the supplementary angle of incident angle. Thus, the ULA has an aliasing problem.

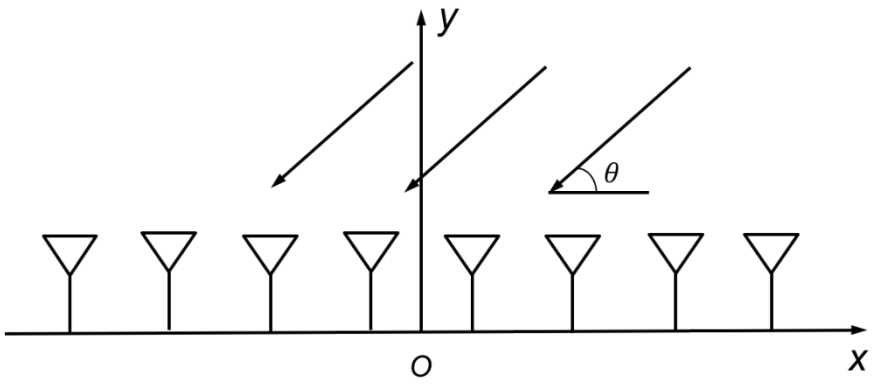

Figure 3. Uniform linear array.

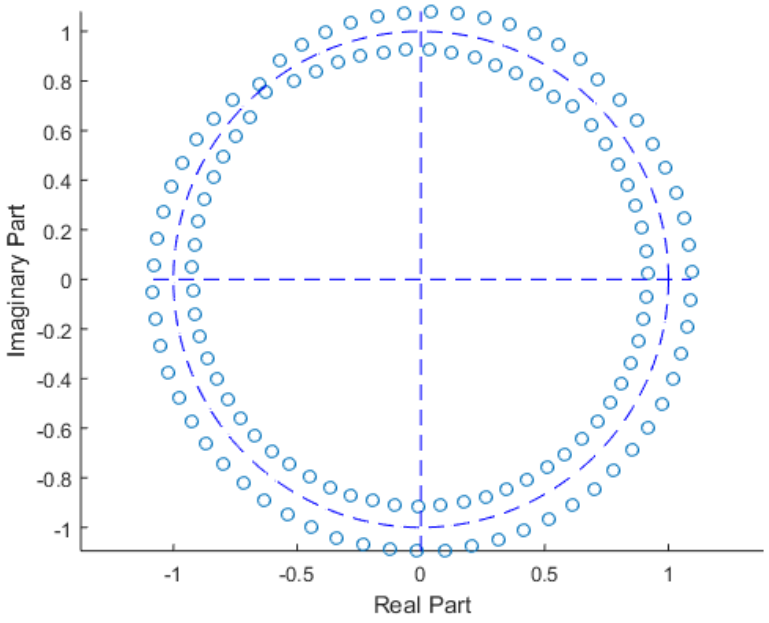

Figure 4. Roots of the polynomial for ULA.

Table 1. Incident and simulated angle for ULA

Incident Angle	Simulated Angle
50 °	130 °

Then, FD Root-MUSIC is used to examine the DOA in NUA, which does not have the aliasing problem. The roots of polynomial are shown in Figure 5, the results are shown in Table 2.

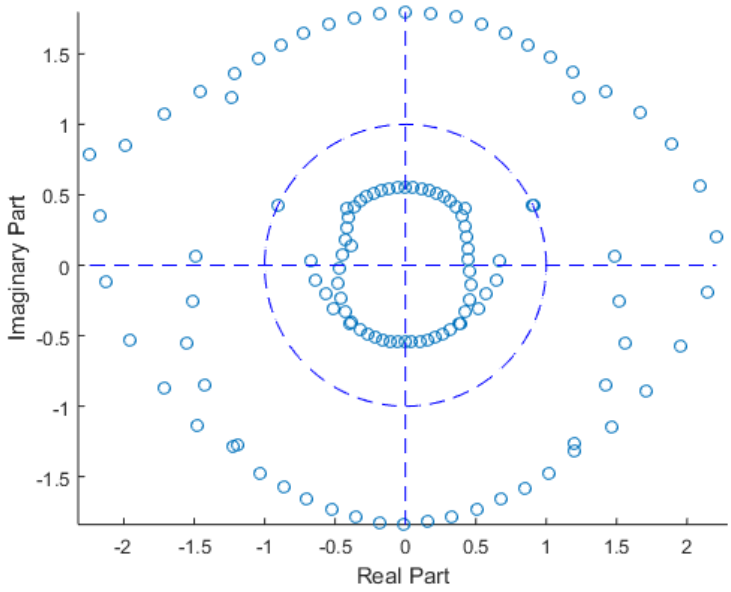

Figure 5. Roots of the polynomial for NUA.

Table 2. Incident and simulated angle for NUA

Incident Angle	Simulated Angle
25 °	24.9972 °

Then, take the spherical array as an example. Twenty-five elements are located in a sphere which is shown in Figure 6. The results are shown in Table 3. The estimated angles are very accurate. Figure 7 shows a volumetric random array. Sixteen elements are randomly located in a sphere with radius 380mm. Table 4 gives the estimated angles and incident angles, which shows that the results are very accurate. Furthermore, there is no aliasing problem in the 3D arrays.

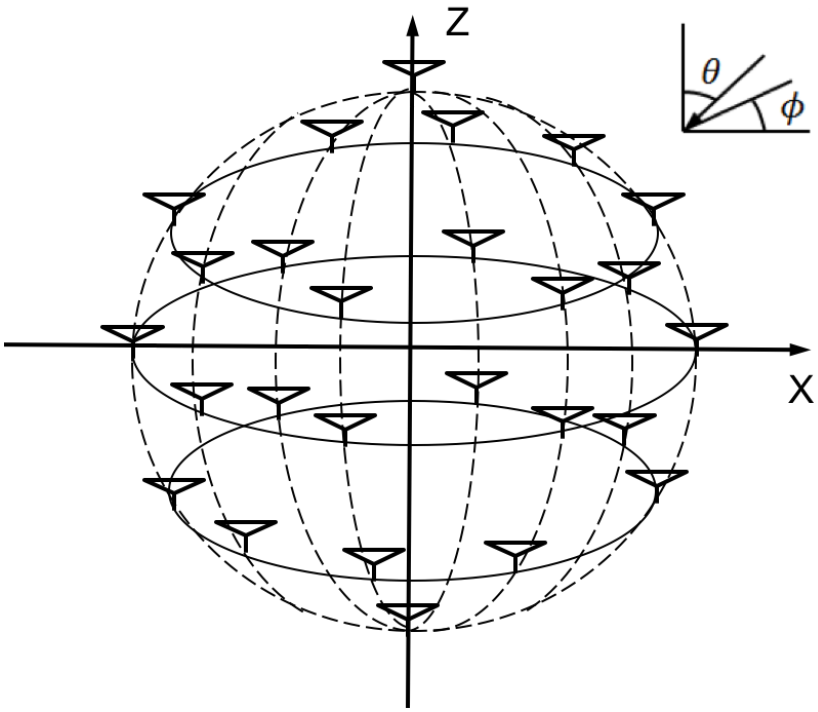

Figure 6. Spherical array structure.

Table 3. Incident and simulated angle for spherical array

Simulation Results of DOA Estimation for Spherical Arrays					
Incident Signal		Estimated DOA		Error	
Azimuth	Elevation	Azimuth	Elevation	Azimuth	Elevation
90°	170°	89.911°	170°	0.089°	0°
60°	140°	59.9995°	140°	0.0005°	0°

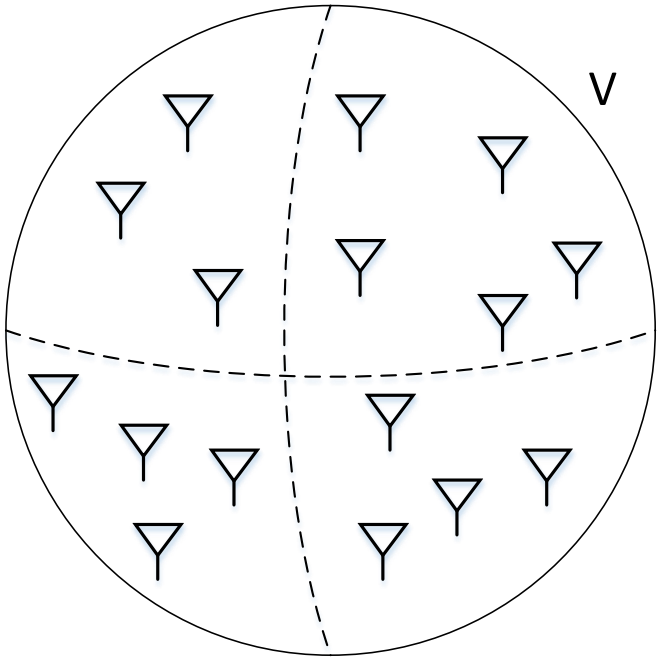

Figure 7. Volumetric random array structure.

Table 4. Incident and simulated angle for volumetric random array

Simulation Results of DOA Estimation for Volumetric Random Array					
Incident Signal		Estimated DOA		Error	
Azimuth	Elevation	Azimuth	Elevation	Azimuth	Elevation
90°	170°	89.9363°	170°	0.0637°	0°
60°	140°	59.9818°	140°	0.0182°	0°

2.3.4 Contrast of Computational Complexity

This section talks about the contrast of the computational complexity of MUSIC and FD Root-MUSIC algorithm. First, assume that N is the number of receiving elements, D is the number of incident signals, J is the total number of spectral points, M is the degree of FD Root-MUSIC polynomials, and $J>>N$, $J>>M$. The contrast of computational complexity of MUSIC and FD Root-MUSIC algorithm is shown in Table 5. According to the computational complexity, different scenarios provide different trade-offs. When the $M << N$, the FD Root-MUSIC algorithm reduces the complexity significantly.

Table 5. Contrast of computational complexity

Algorithm	Computational Complexity
Spectral MUSIC	$O(N^3 + JND)$
FD Root-MUSIC	$O(N^3 + MND + M\log_2 M + \text{degree} - M\,rooting)$

3. IMPACT OF UAV SWARM DENSITY AND HETEROGENEITY ON SYNTHETIC APERATURE DOA CONVERGENCE

3.1 Introduction

This section comes up with a creative method to utilize swarming UAVs which morph over time to create unstructured morphing antenna arrays as a distributed data collection system. The position and orientation of the UAVs are altered over time to create a synthetic aperture. This work proposes a mathematic model of the data collection system and evaluates the performance of the system. According to the model, simulations are used to investigate the impact of the UAV swarm density and heterogeneity derived from rotated pattern functions.

3.2 Swarming UAV Synthetic Aperture

The swarming UAV synthetic aperture was first introduced in [24]. Figure 8 is a schematic diagram of a UAV swarm morphing in time. Assume that there are *M* UAVs and each of them has a position, orientation, and trajectory. Suppose that these UAVs have position $P_{n,t}(r,\theta,\phi)$, where *n* is the UAV's index and *t* is the 'snapshot' time parameter. It is convenient to use a dual quaternion framework to handle the UAV swarming behavior, where the UAVs undergo rotations and translations during swarming. Therefore, the swarming process alters the antenna radiation pattern's spatial orientation with respect to the global coordinate system and incident signals. Each UAV has local (u,v,w) coordinate system shown in the figure. The incident data $S(\theta_0,\phi_0)$ is collected over time and the parameters of interest (θ_0,ϕ_0) can be obtained by the collection of the measurements.

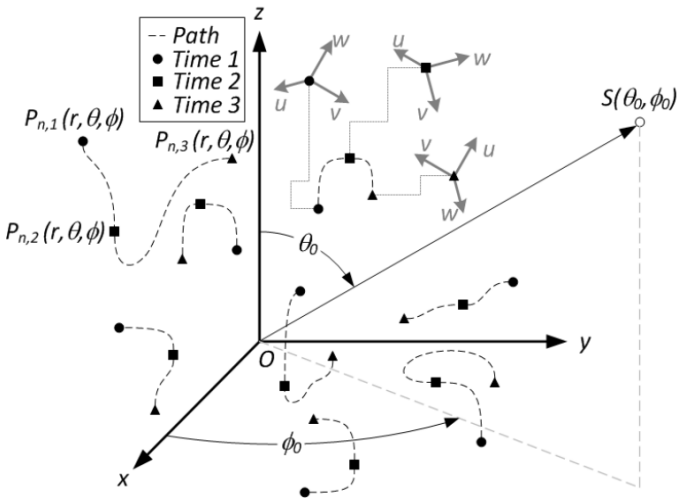

Figure 8. Swarming UAV synthetic aperture reprinted from [24] © 2017 IEEE.

3.3 Swarming Model

In [23], Dr. Friedlander came up with a mutual coupling model, which includes the phase, gain and mutual coupling effects. Refer to the model, assume that N is the number of radiating sources and M is the number of elements in a receiving array. Therefore, the received signals at the *m*th agent can be represented as

$$x_m(t) = \sum_{n=1}^{N} \alpha_m s_n(t - \tau_{mn} - \psi_m) + w_m(t), \quad -T/2 \le t \le T/2, \qquad m = 1, 2, \cdots, M \tag{18}$$

where the mutual coupling effects are not introduced, $\{s_n(t)\}_{n=1}^{N}$ are the radiated signals, $\{w_m(t)\}_{m=1}^{M}$ are the additive noise, and T is the observation period. $\{\tau_{mn}\}$ are delays from the *n*th source to the *m*th sensor with respect to the signal propagation time. In the end, α_m and ψ_m are the gain and the delay relative to the *m*th sensor.

It is convenient to use Fourier coefficients to separate the parameters. It can be defined by

$$X_m(\omega_l) = \frac{1}{\sqrt{T}} \int_{-T/2}^{T/2} x_m(t) e^{-j\omega_l t} dt \tag{19}$$

where $\omega_l = 2\pi(l_1 + l)/T$, $l = 1, 2, \cdots, L;$ and l_1 is a constant. The number of coefficients should be infinite to get all the signal information in theory. But, the signals we are interested in are narrow-band. Assume the spectrum is concentrated around ω_0, and the bandwidth is small relative to $2\pi / T$. Thus, L=1. Recall the Fourier coefficients of (8) on ω_0, we obtain

$$X_m = \sum_{n=1}^{N} \alpha_m e^{-j\omega_0 \psi_m} \cdot e^{-j\omega_0 \tau_{mn}} S_n + W_n \qquad m = 1, 2, \cdots, M \tag{20}$$

where S_n and W_n are the Fourier coefficients of $s_n(t)$ and $w_m(t)$, respectively. The α_m and ψ_m change with respect to element location based on orientation of UAV; τ_{mn} changes with respect to location; S_n is constant; W_n may change with respect to location, velocity of UAV, and environment. Equation (10) can be represented by

$$X(k) = \Gamma \cdot \mathrm{A} \cdot S(k) + W(k); \qquad k = 1, 2, \cdots, K \tag{21}$$

where *k* is the index of different (independent) samples and

$$X(k) = [X_1(k), X_2(k), \cdots, X_M(k)]^T,$$

$$S(k) = [S_1(k), S_2(k), \cdots, S_N(k)]^T,$$

$$W(k) = [W_1(k), W_2(k), \cdots, W_M(k)]^T,$$

$$\Gamma = diag\{\alpha_1 e^{-j\omega_0 \psi_1}, \alpha_2 e^{-j\omega_0 \psi_2}, \cdots, \alpha_M e^{-j\omega_0 \psi_M}\},$$

$$A_{mn} = e^{-j\omega_0 \tau_{mn}} \quad m = 1, 2, \cdots, M; \quad n = 1, 2, \cdots, N.$$

Here we consider the sources are in the far field from the observing array. It is easy to find that τ_{mn} can be represented by

$$\begin{aligned} &\tau_{mn} = -d_{mn} / c, \\ &d_{mn} = x_m \sin\theta_n \cos\phi_n + y_m \sin\theta_n \sin\phi_n + z_m \cos\theta_n \end{aligned} \tag{22}$$

where d_{mn} is the distance from origin (reference sensor) of the coordinate to the sensor *m* in the direction of *n*th source, *c* is the propagating velocity in free space, (x_m, y_m, z_m) are the coordinates of the *m*th sensor, (θ_n, ϕ_n) are the DOA of *n*th source in the sphere coordinate. Figure 9 shows the geometry of one UAV swarming 8 times in the Cartesian coordinate system.

From equations (11) and (12), the matrix *A* can be obtained by

$$A_{mn} = e^{j(\omega_0 / c)(x_m \sin\theta_n \cos\phi_n + y_m \sin\theta_n \sin\phi_n + z_m \cos\theta_n)} \tag{23}$$

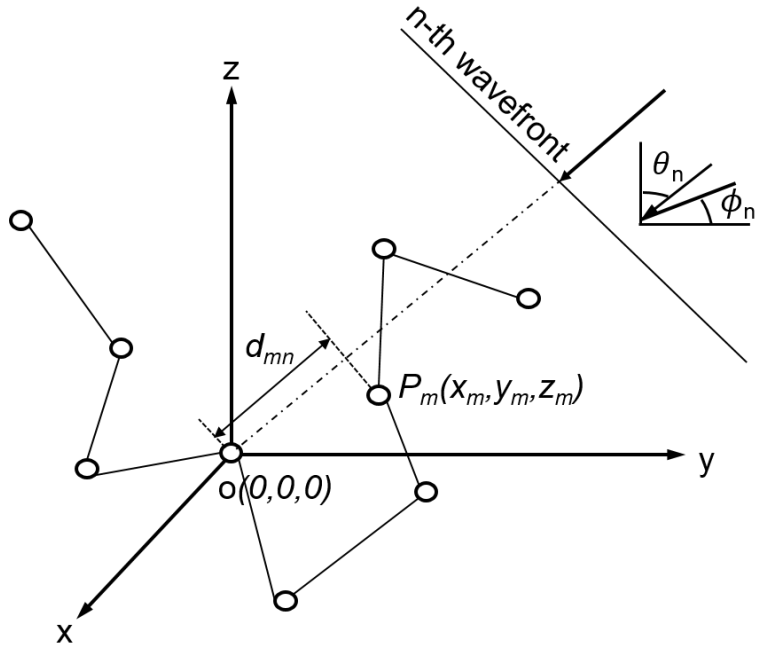

Figure 9. Geometry for one UAV morphing 8 times with the n-th wavefront.

3.3.1 UAV Parameters

Each UAV swarms in a cylinder region ($r=\lambda$, 10λ, or 100λ, h= 2r, λ is wavelength and λ = 1000mm). Each UAV has an initial location (x, y, z) in the swarming region with a vector velocity $\vec{V}_m$. The swarming short distance at each iteration is a vector $\vec{d}_m$. The scalar quantity in the x, y, and z direction can be represented as *dx*, *dy* and *dz*, which uses the following relation:

$$\begin{aligned} d_x &= \beta_t \cdot 0.4\lambda + 0.1\lambda, \quad d_x \in (0.1\lambda, 0.5\lambda) \\ d_y &= \beta_t \cdot 0.4\lambda + 0.1\lambda, \quad d_y \in (0.1\lambda, 0.5\lambda) \\ d_z &= \beta_t \cdot 0.4\lambda + 0.1\lambda, \quad d_z \in (0.1\lambda, 0.5\lambda) \end{aligned} \tag{24}$$

where β_t is a uniformly distributed random number between zero and one. We also can obtain:

$$\vec{d}_m = \vec{V}_m \cdot t \tag{25}$$

3.3.2 Data Processing and Algorithm

When the UAV swarms, there will be a lot of data information due to the number of iterations. There are several ways to process the data:

1) Only use the current data to calculate the MUSIC spectrum
2) Use current data and all previous data to calculate the MUSIC spectrum
3) Use current and some previous data to calculate the MUSIC spectrum

One of the benefits using the swarm system is to use the previous data to increase the performance of DOA convergence, so the benefits will be gone if the previous data are not utilized. However, if all the previous data are accumulated to calculate the MUSIC spectrum, the data matrix will be very big and the computational complexity will be super high. So, it is necessary to compromise the previous data usage and computational complexity. Here we take the type 3 to investigate the performance.

Another problem is how many data points should be used to calculate the MUSIC spectrum at each iteration. Since more data points for MUSIC spectrum calculation each time means more array elements using for data collecting in an antenna array, and more accurate for DOA estimation. However, more data processing points cause higher calculation cost. Thus, it is necessary to compromise the number of data points at each MUSIC spectrum calculation and computational complexity. Based on type 3, 6 data points, 10 data points, 100 data points and even more data points can be used to calculate

the MUSIC spectrum at each iteration. I will talk about the impact of different type of data sets at each iteration later. Here, we take 10 data points for each group.

Figure 10 shows the data processing schematic for 6 data points each set in the UAV swarm system. When UAV swarms to a certain location, we will sample 5 times (5 snapshots) and each snapshot takes the time d_t. After taking 5 snapshots, the program sets up a data point. After the number of data points $N_d = 6$, the program calculates the MUSIC spectrum and stores the result. Then UAV swarms again, we accumulate current data and previous data to calculate the MUSIC spectrum. Furthermore, we multiply the current MUSIC spectrum and previous MUSIC spectrum at each iteration where we obtain the MUSIC spectrum to reduce the noise level and improve the DOA performance. Note that if the iteration is too big, the value of the spectral points will be very small and might be taken as zero. If so, the correct DOA cannon be obtained. We should use dB instead of number at that situation.

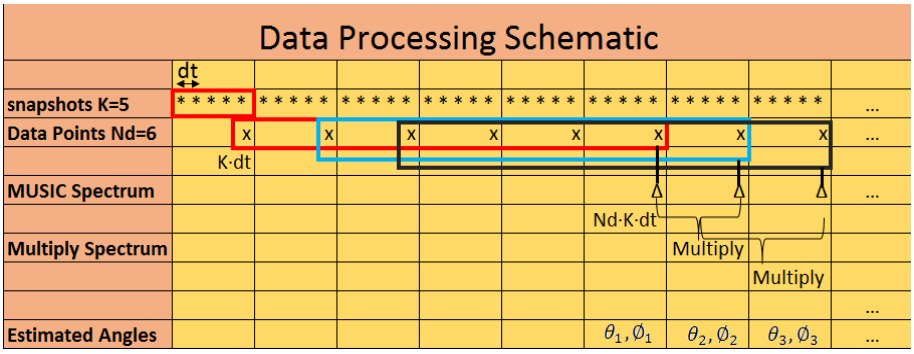

Figure 10. Data processing schematic for UAV swarm system.

Consider the two problems above, the steps of the algorithm are:

Step 1: UAV swarms until the number of the data is 12, then, calculate the MUSIC spectrum;

Step 2: UAV swarms again, and use current data and previous data to calculate the MUSIC spectrum at each iteration;

Step 3: Multiply the current MUSIC spectrum and previous spectrum

Step 4: Repeat step 2-3 until the swarming system converges

The algorithm flow chart is shown in Figure 11.

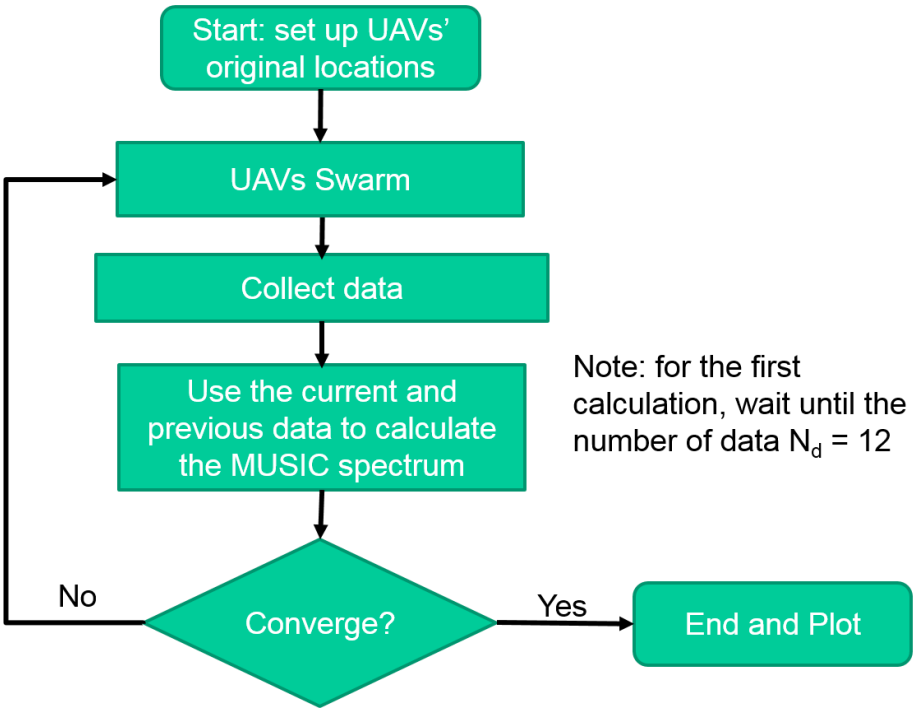

Figure 11. Flow chart of the algorithm.

3.3.3 Convergence Check

The algorithm performs the calculation until the system converges. The convergence can be guaranteed, since the estimated DOA is a convergent series.

When the signal is covered by a high noise level, the estimated DOA might be far from the ground truth and cannot be judged for the convergence. But as the iteration increases, the noise level is reduced and the estimated DOA is converged gradually. Avoiding the misjudgment, the equation for judging the convergence is given by

$$DOA_n - \sum_{m=1}^{10} DOA_{n-m} < \varepsilon, \quad n = 1, 2, \cdots t \tag{26}$$

where t is the number of iteration and ε is the preset threshold.

3.4 Example and Performance for One UAV Swarm

If there is only one source and one UAV at time t_1, (8) can be given by

$$X_1(t) = \alpha_1(t) e^{-j\omega_0 \psi_1(t)} \cdot e^{-j\omega_0 \tau_{11}(t)} S_1 + W_1(t) \tag{27}$$

where subscript "1" represents UAV number one; α_1 and ψ_1 may change with respect to element location based on orientation of UAV; τ_{11} changes with respect to location; S_1 is constant; W_1 may change with respect to location, velocity of UAV, and environment.

First, consider the ideal case: one UAV swarms without rotating at the cylinder region ($r=\lambda$, $h=2\lambda$), so the array constructed by the swarming system is identical, which gives $\Gamma_1 = 1$. Assume the $SNR = 0$, the snapshot $K = 5$, it is a very noisy condition. Choose 200 iterations (enough for us to examine the performance) for one UAV swarming at one pass and keep the short distance as $dx \in (0.1\lambda, 0.5\lambda)$, $dy \in (0.1\lambda, 0.5\lambda)$, $dz \in (0.03\ \lambda, 0.43\lambda)$.

The diagram is shown in Figure 12. Figure 13 shows the simulated azimuth and elevation errors, Figure 14-17 show the simulated two-dimension (2D) and three-dimension (3D) MUSIC spectrum with iteration increasing. Then, Figure 18 shows the average of azimuth and elevation errors with ten passes.

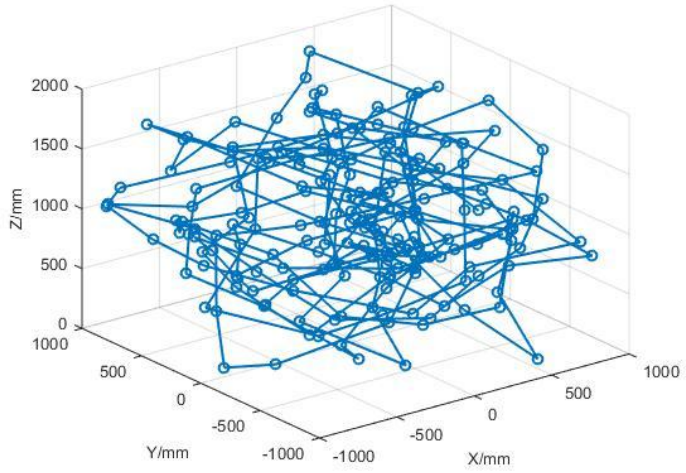

Figure 12. Diagram of one UAV swarming with number of iteration t = 200, density of swarming region $r = 1\lambda$.

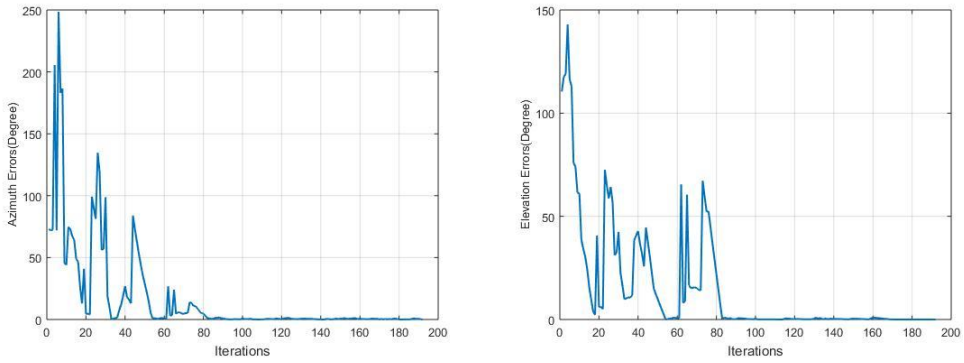

Figure 13. Simulated DOA errors of an incident signal with an azimuth of 60° and elevation of 120°.

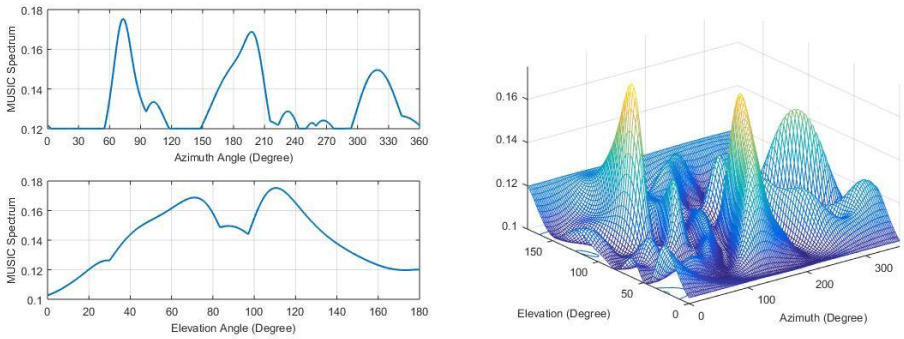

Figure 14. Simulated MUSIC spectrum with number of iteration t = 1, an incident signal with an azimuth of 60° and elevation of 120° .

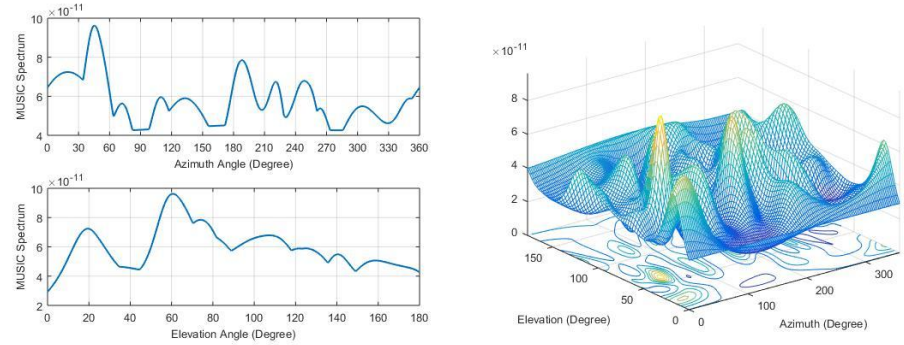

Figure 15. Simulated MUSIC spectrum with number of iteration t = 11, an incident signal with an azimuth of 60° and elevation of 120° .

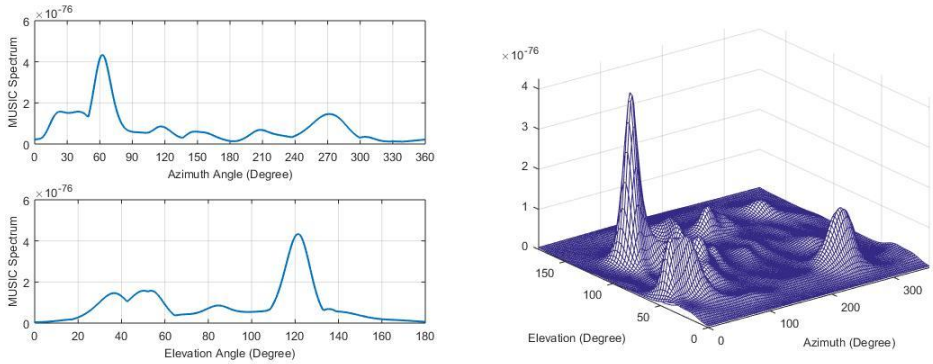

Figure 16. Simulated MUSIC spectrum with number of iteration t = 81, and DOA of an azimuth of 60° and elevation of 120° .

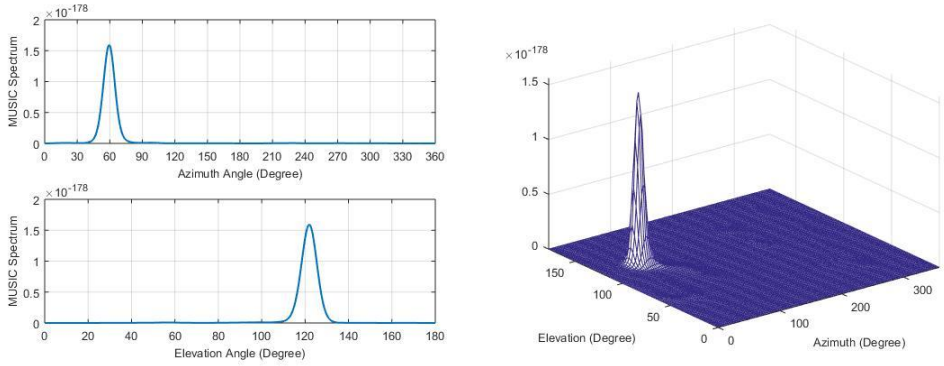

Figure 17. Simulated MUSIC spectrum with number of iteration t = 191, and DOA of an azimuth of 60° and elevation of 120°.

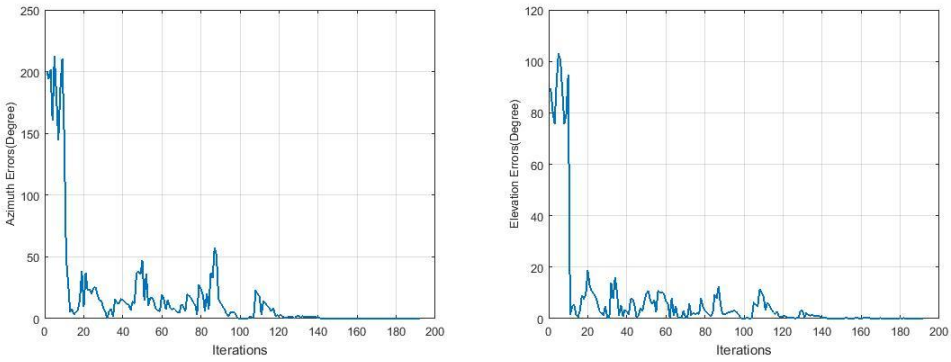

Figure 18. Simulated average of azimuth and elevation errors of ten passes with number of iteration t = 200, and DOA of an azimuth of 60° and elevation of 120°.

Results above show that one UAV swarm system in the ideal case converges very fast.

3.5 Impact Factors for DOA Convergence in the UAV Swarming System

The convergence of a DOA estimation technique depends on a number of parameters. The scope, dependence, and complexity of these parameters changes significantly when a UAV swarm is used as the data collection platform. Key parameters for this include the total number of UAVs collecting data, the density (or number of data

collectors in a given region) that are swarming, each UAV's velocity in the swarm, and the phase errors due to noise, interference, and a host of other uncertainties. A series of numerical simulations are presented in this section to observe the impact of these parameters – fixing some while varying others. All results provided in this section represent the average of ten simulation runs and each run of these simulations has an iteration count t = 500. The parameters varied are:

- Number of UAVs: M = 1,10
- Number of data processing points: N_d = 1, 10, 100, and 500
- Number of snapshots: K = 1,10, and 100
- Swarming range: r = 1,10, and 100 λ
- Velocity v (represented by the distance): d = 0.1~0.5 λ , etc.
- SNR = -20, 0, and 20 dB
- Phase errors due to environment and UAV rotation

3.5.1 Impact of Number of UAVs

When there is more than one UAV morphing at the same time, the antenna array will change fast at each iteration. Let the number of iterations t = 500, the number of data processing points N_d =10, snapshots K=5, swarming range r =1λ, distance $d\in$ (0.1λ, 0.5λ), SNR = 0 dB, phase error = 0. The number of UAVs varies at 1 and 10. Figure 19-22 show that the swarming system will converge faster when the number of the UAVs are increased.

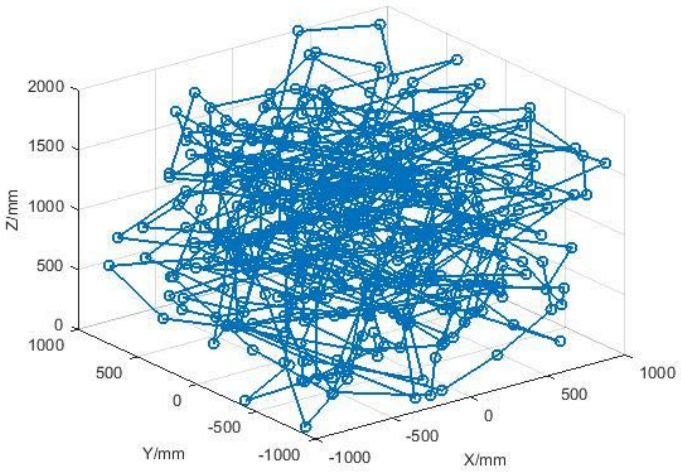

Figure 19. Diagram of one UAV swarming for 500 iterations with different number of UAVs.

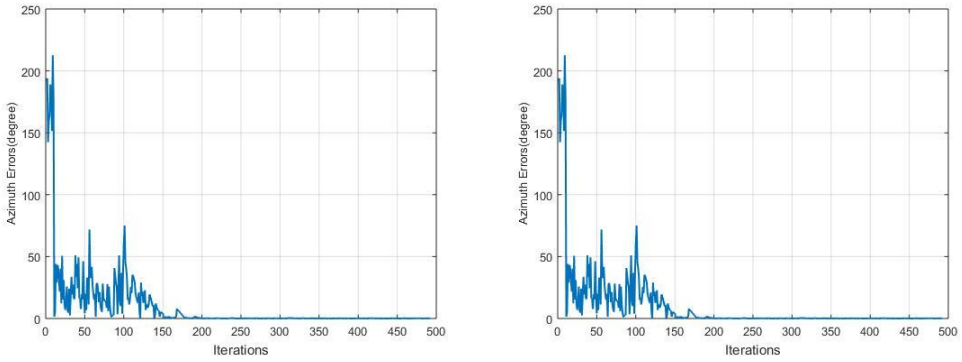

Figure 20. Simulated average of azimuth and elevation errors of ten passes with number of UAVs $M = 1$, and DOA of an azimuth of 60° and elevation of 120°.

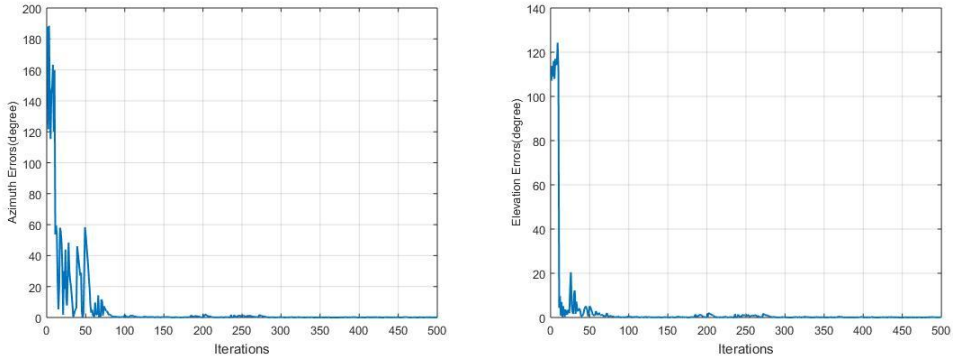

Figure 21. Simulated average of azimuth and elevation errors of ten passes with number of UAVs M = 10, and DOA of an azimuth of 60° and elevation of 120°.

3.5.2 Impact of Number of Data Processing Points

The number of data processing points at each iteration corresponds to the number of elements in an antenna array without time-varying. Thus, it is very important to decide how many data points should be utilized to calculate the MUSIC spectrum and estimation DOA.

Choose the number of data points at each group N_d = 10, 100. We already know that when N_d = 10, it can be converged well in the section 3.5.1. In this section, one UAV swarm are used to investigate the impact factors. Let the number of iterations t = 500, the number of UAVs M = 1, snapshots K=5, swarming range r =1λ, distance $d \in$ (0.1λ, 0.5λ), SNR = 0 dB, phase error = 0. The number of data processing points varies at 6, 10, and 100. Figure 22 shows that when the N_d = 6, it is not easy to converge. Figure 4 shows that when N_d = 100, it converges very fast. The results about N_d = 10 is shown in Figure 20.

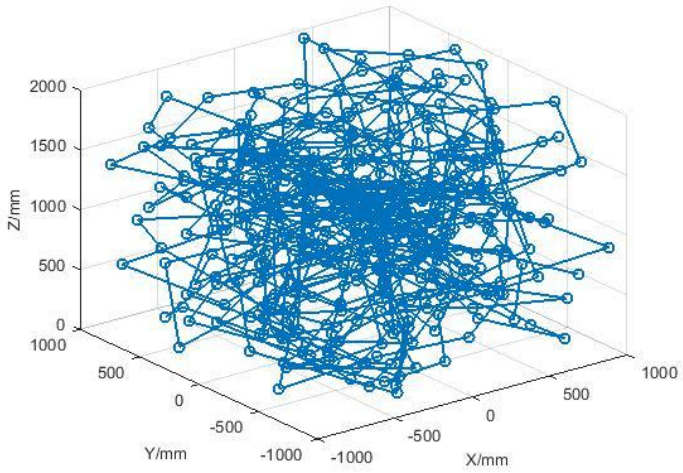

Figure 22. Diagram of one UAV swarming for 500 iterations with different data points.

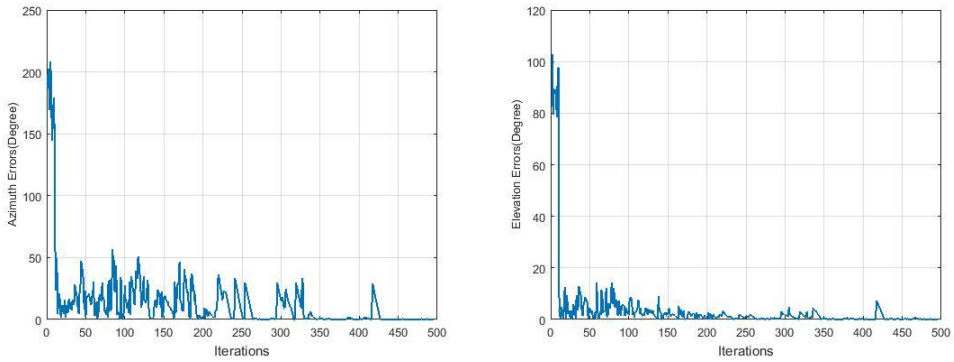

Figure 23. Simulated average of azimuth and elevation errors of ten passes with number of data points N_d = 6, and DOA of an azimuth of 60° and elevation of 120°.

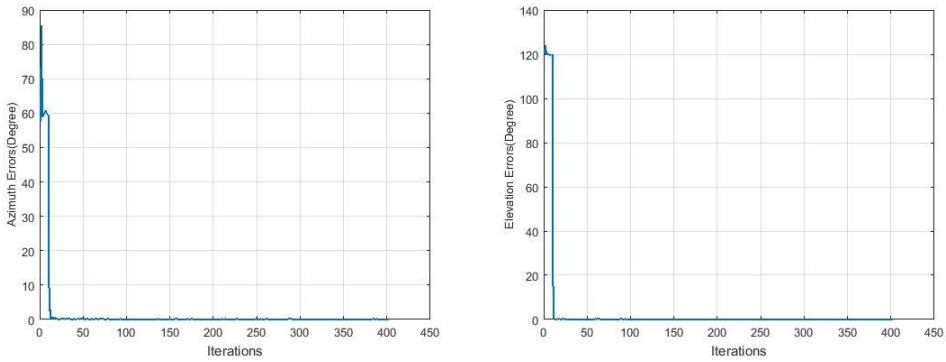

Figure 24. Simulated average of azimuth and elevation errors of ten passes with number of data points N_d = 100, and DOA of an azimuth of 60° and elevation of 120°.

3.5.3 Impact of Snapshots

When the snapshots are increased, obviously the noise would be reduced. Let the number of iterations t = 500, the number of UAVs M = 1, the number of data processing points N_d =10, swarming range r =1λ, distance $d \in (0.1\lambda, 0.5\lambda)$, SNR = 0 dB, phase error = 0. The number of snapshots K varies at 1, 10 and 100. Figure 26-27 show that the noise will be reduced faster when the number of the UAVs are increased.

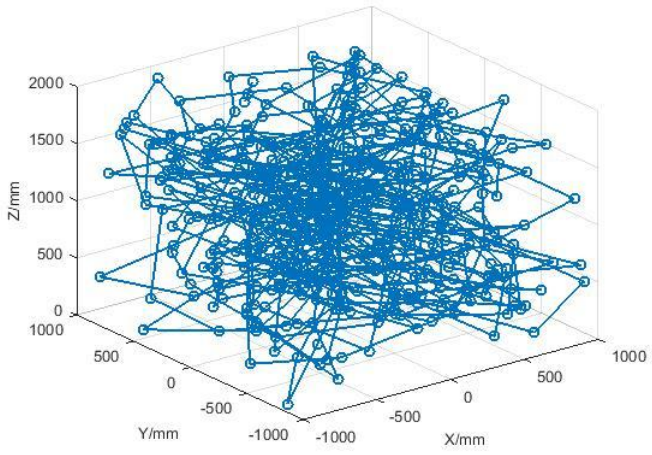

Figure 25. Diagram of one UAV swarming for 500 iterations with different snapshots.

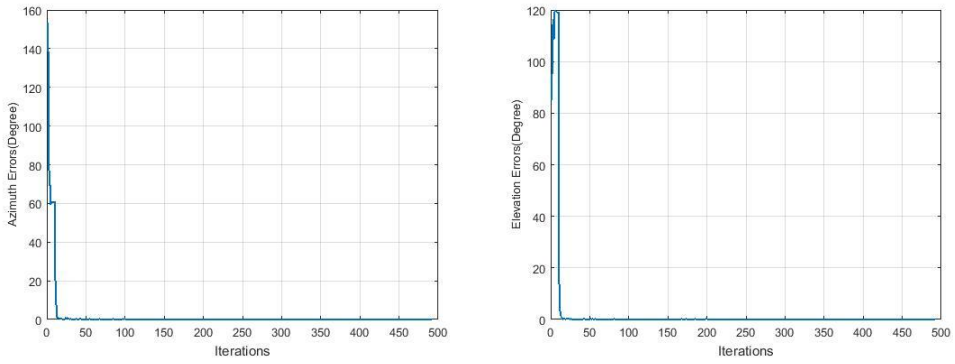

Figure 26. Simulated average of azimuth and elevation errors of ten passes with number of snapshot K = 10, and DOA of an azimuth of 60° and elevation of 120°.

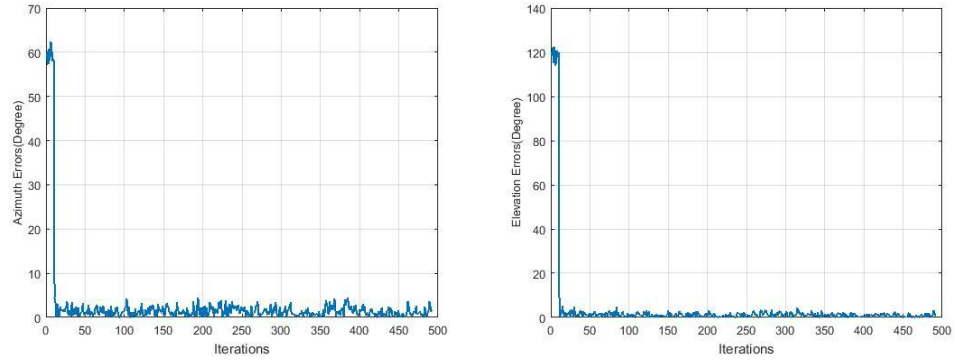

Figure 27. Simulated average of azimuth and elevation errors of ten passes with number of snapshots K = 100, and DOA of an azimuth of 60° and elevation of 120°.

3.5.4 Impact of SNR

When the *SNR* are increased, the noise level is reduced. Let the number of iterations t = 500, the number of UAVs M = 1, the number of data processing points N_d =10, snapshots K = 5, swarming range r =1λ, distance $d \in (0.1\lambda, 0.5\lambda)$, phase error = 0. The *SNR* varies at -20, 0 and 20 dB. Figure 19-30 show that the impact of *SNR*.

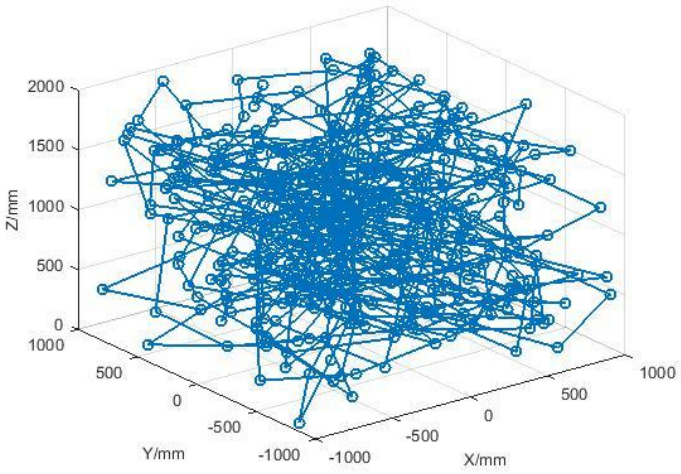

Figure 28. Diagram of one UAV swarming for 500 iterations with different SNR.

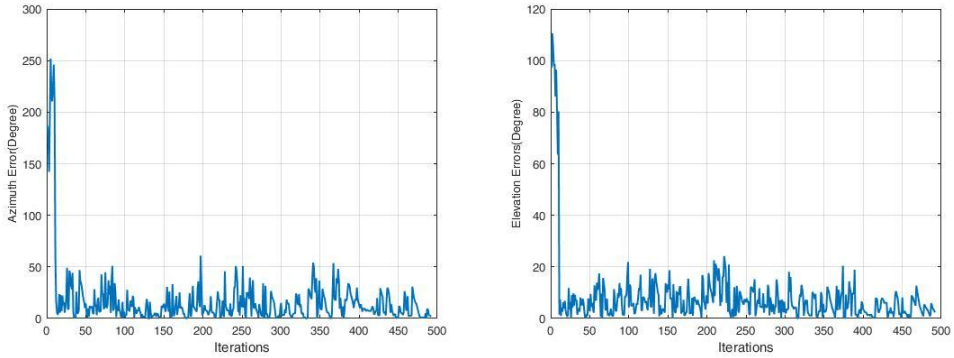

Figure 29. Simulated average of azimuth and elevation errors of ten passes with *SNR* = -20 dB, and DOA of an azimuth of 60° and elevation of 120°.

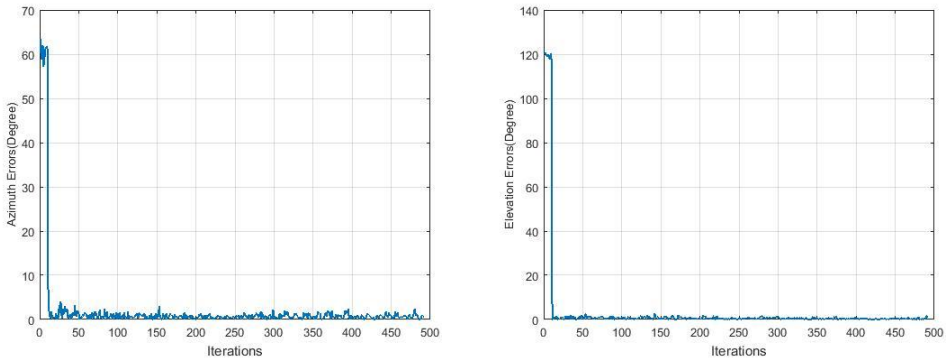

Figure 30. Simulated average of azimuth and elevation errors of ten passes with *SNR* = 20 dB, and DOA of an azimuth of 60° and elevation of 120°.

3.5.5 Impact of Swarming Density and UAV Velocity

This section first discusses about the impact of swarming density, and then talks about the impact of UAV velocity related to the wavelength. Bigger swarming region will bring in more noise. The UAV velocity related to the short distance at each iteration will change the array structure, and thus impact the DOA convergence. When the short distance is too small between 0.05 λ and 0.1 λ, the estimated arrival angle even cannot be converged. When the short distance is too big between 10 λ and 30 λ, the estimated arrival angle will be converged more slowly. Thus, the distance cannot be too small or too big, it should be suitable with respect to the wavelength to create a good antenna array structure. First, let the $dx \in (0.1\ \lambda, 0.5\lambda)$, dy $(0.1\ \lambda, 0.5\lambda)$, $dz \in (0.03\ \lambda, 0.43\lambda)$, and vary swarming region at $r = 1\lambda$, 10λ, and 100λ. Figure 20 and Figure 31-34 show the impact of swarming density from $r = 1\lambda$ to $r = 100\lambda$. Then, let the swarming region $r = 10\ \lambda$, and 100λ, vary the short distance d from $dx \in (0.1\ \lambda, 0.5\lambda)$ to $dx \in (10\ \lambda, 50\lambda)$ to examine the impact of the UAV velocity. Figure 35-42 show the numerical simulation results.

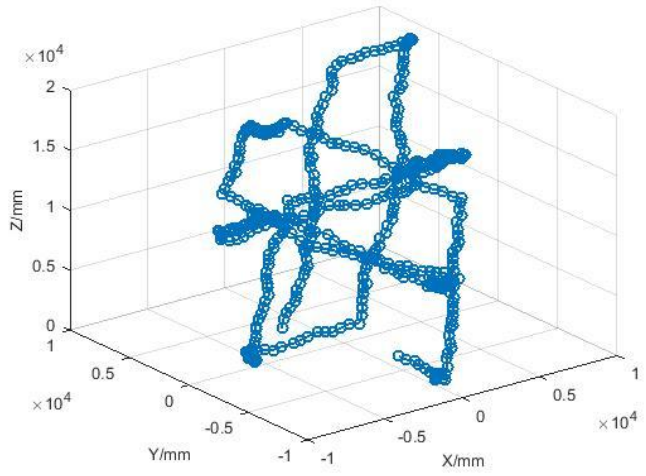

Figure 31. Diagram of one UAV swarming with number of iteration t = 500, swarming region r = 10 λ, and short distance $dx \in (0.1\ \lambda, 0.5\lambda)$, $dy \in (0.1\ \lambda, 0.5\lambda)$, $dz \in (0.03\ \lambda, 0.43\lambda)$.

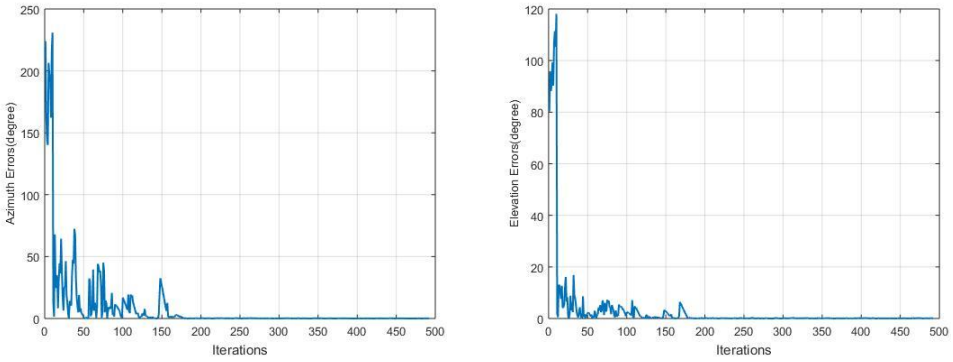

Figure 32. Simulated average of azimuth and elevation errors of ten passes with swarming region r = 10λ, short distance $dx \in (0.1\ \lambda, 0.5\lambda)$, $dy \in (0.1\ \lambda, 0.5\lambda)$, $dz \in (0.03\ \lambda, 0.43\lambda)$ and DOA of an azimuth of 60° and elevation of 120° .

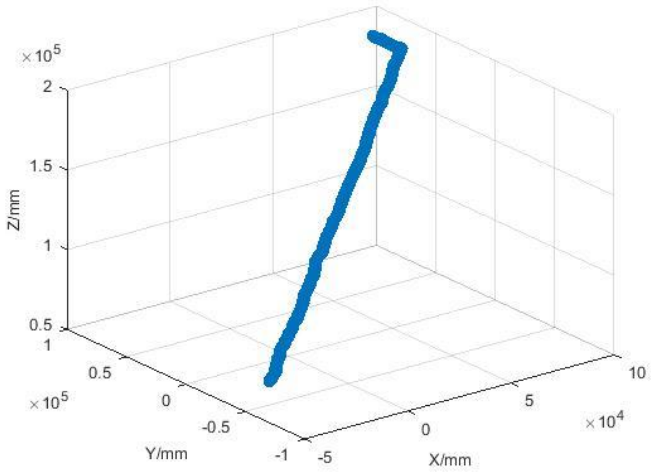

Figure 33. Diagram of one UAV swarming with number of iteration t = 500, swarming region r = 100 λ, and short distance $dx \in (0.1\ \lambda, 0.5\lambda)$, $dy \in (0.1\ \lambda, 0.5\lambda)$, $dz \in (0.03\ \lambda, 0.43\lambda)$.

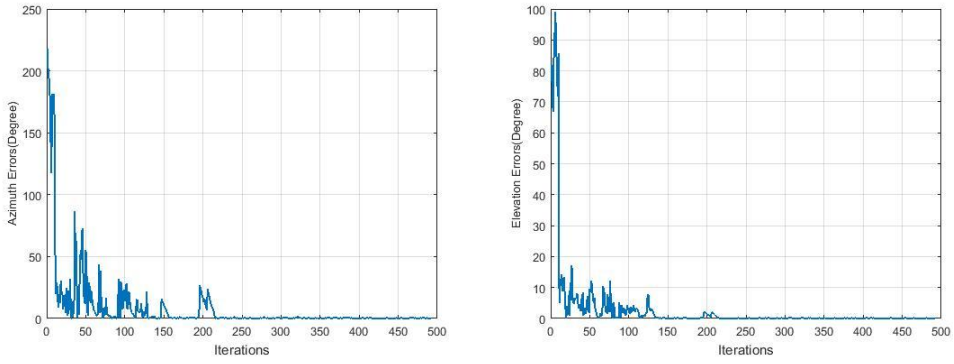

Figure 34. Simulated average of azimuth and elevation errors of ten passes with swarming region r = 100λ, short distance $dx \in (0.1\ \lambda, 0.5\lambda)$, $dy \in (0.1\ \lambda, 0.5\lambda)$, $dz \in (0.03\ \lambda, 0.43\lambda)$ and DOA of an azimuth of 60° and elevation of 120° .

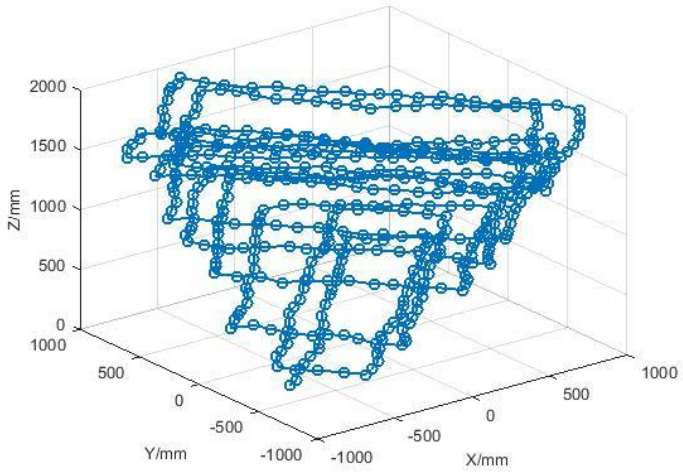

Figure 35. Diagram of one UAV swarming with number of iteration t =500, swarming region r = 1 λ, and short distance $dx \in (0.05\,\lambda, 0.1\lambda)$, $dy \in (0.05\lambda, 0.1\lambda)$, $dz \in (0.05\lambda, 0.1\lambda)$.

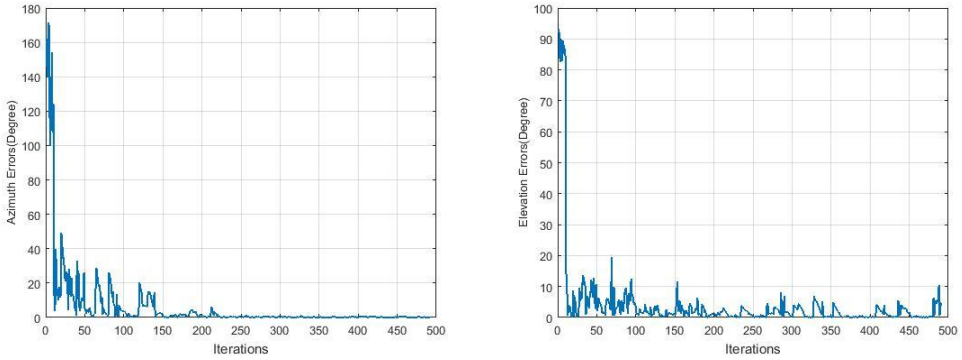

Figure 36. Simulated average of azimuth and elevation errors of ten passes with swarming region r = 1λ, short distance $dx \in (0.05\,\lambda, 0.1\lambda)$, $dy \in (0.05\,\lambda, 0.1\lambda)$, $dz \in (0.05\lambda, 0.1\lambda)$ and DOA of an azimuth of 60° and elevation of 120° .

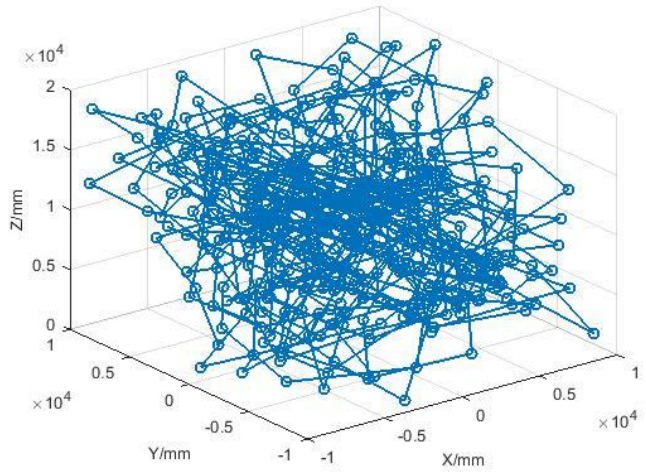

Figure 37. Diagram of one UAV swarming with number of iteration t =500, swarming region r = 10λ, and short distance $dx \in (1\lambda,5\lambda)$, $dy \in (1\lambda,5\lambda)$, $dz \in (0.93\lambda,4.93\lambda)$.

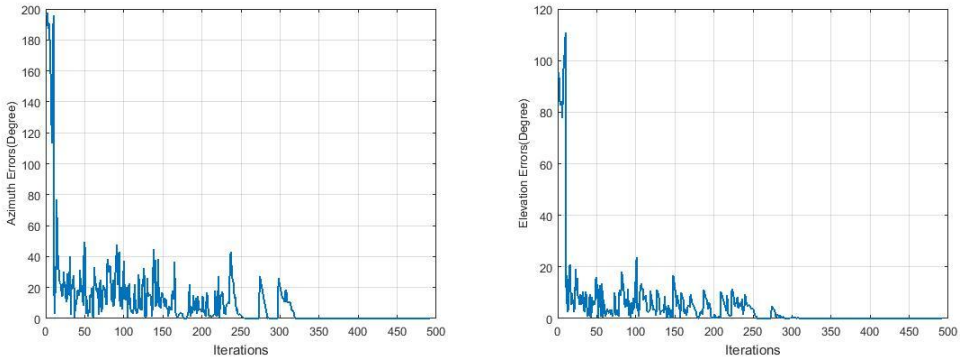

Figure 38. Simulated average of azimuth and elevation errors of ten passes with swarming region r = 10 λ, and short distance $dx \in (1\lambda,5\lambda)$, $dy \in (1\lambda,5\lambda)$, $dz \in (0.93\lambda,4.93\lambda)$ and DOA of an azimuth of 60° and elevation of 120°.

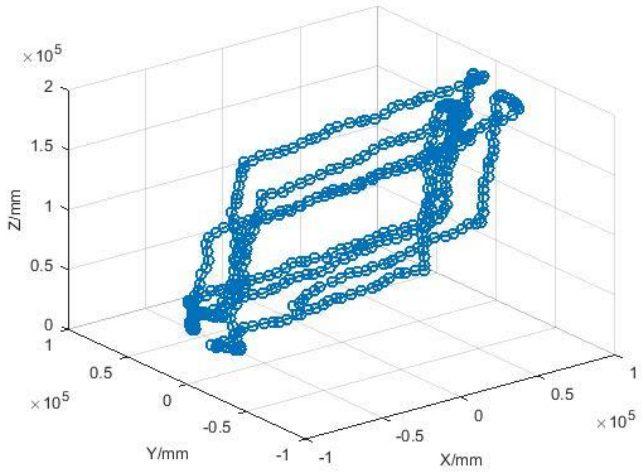

Figure 39. Diagram of one UAV swarming with number of iteration t = 500, swarming region r= 100λ, and short distance $dx \in (1\lambda,5\lambda)$, $dy \in (1\lambda,5\lambda)$, $dz \in (0.93\ \lambda,4.93\lambda)$.

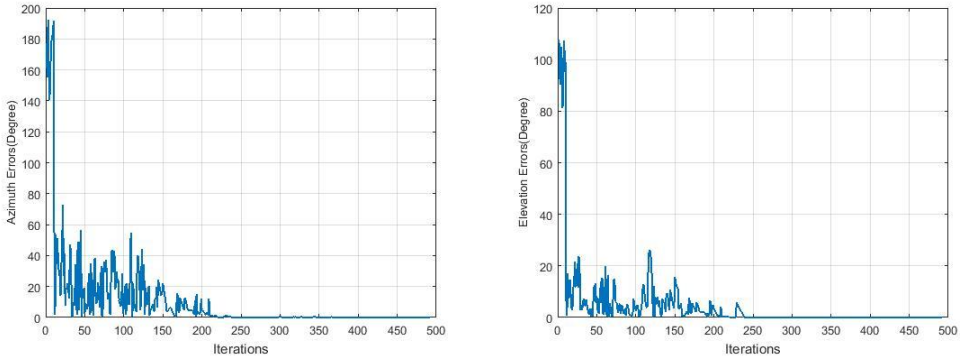

Figure 40. Simulated average of azimuth and elevation errors of ten passes with swarming region r = 100λ, short distance $dx \in (1\lambda,5\lambda)$, $dy \in (1\lambda,5\lambda)$, $dz \in (0.93\ \lambda,4.93\lambda)$, and DOA of an azimuth of 60° and elevation of 120° .

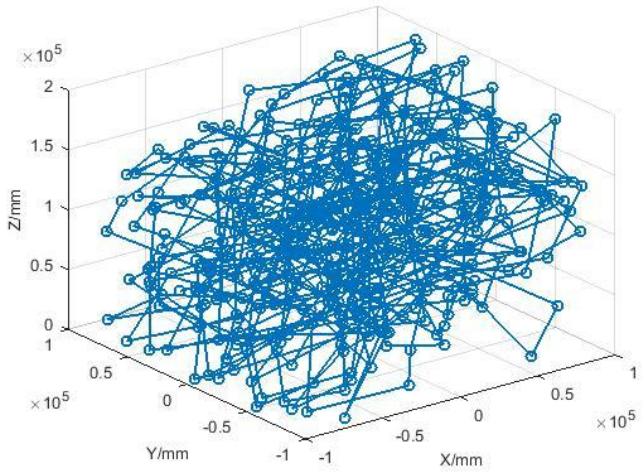

Figure 41. Diagram of one UAV swarming with number of iteration t = 500, swarming region $r = 100\lambda$, and short distance $dx \in (10\lambda,50\lambda)$, $dy \in (10\lambda,50\lambda)$, $dz \in (9.93\ \lambda,49.93\lambda)$.

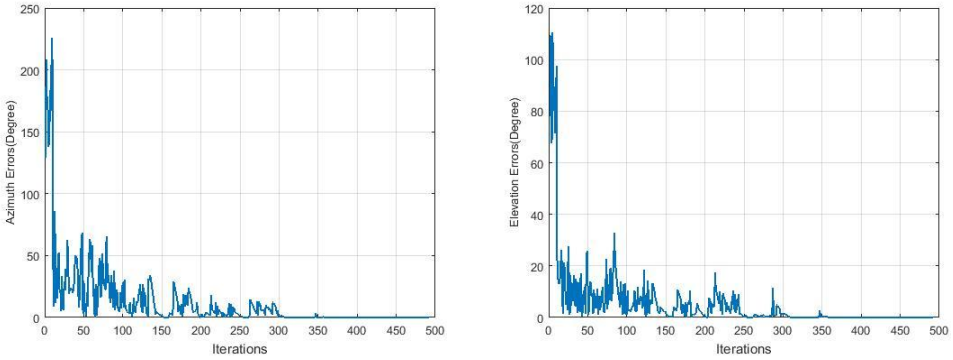

Figure 42. Simulated average of azimuth and elevation errors of ten passes with density of swarming region $r = 100\lambda$, short distance $dx \in (10\lambda,50\lambda)$, $dy \in (10\lambda,50\lambda)$, $dz \in (9.93\ \lambda,49.93\lambda)$ and DOA of an azimuth of 60° and elevation of 120°.

3.6 Impact of Phase Errors

This section introduces two types of distribution, uniformly distribution and normal distribution, for phase errors. In practice, the measured phase difference may have some errors due to the antenna shielding between each other and the UAV rotation as it

swarms. For one UAV swarm system, the shielding error is zero, and even for two or three UAV swarm systems, the shielding errors might be ignored. However, if there are 10, and even 100 UAVs swarming at the same time, the shielding errors would be increased. When the UAV rotates, the received antenna gain and phase would be different and it will cause the phase errors according to the antenna pattern. Some other errors may come from the phase test errors, UAV location test errors, the uncertain environment around the antenna in the UAV (e.g., the effect of metal objects near antenna, and the effect of UAV wings vibrating).

Assume the shielding errors, phase test errors, UAV location errors as the unknown errors $e_{unknown}$, and randomly give the value of $e_{unknown}$ from -5 percent to 5 percent of 2π phase errors. The relation is:

$$e_{unknown} = 2\pi \cdot (\delta_t \cdot 0.1 - 0.05) \tag{28}$$

where δ_t is a uniformly distributed random number between zero and one. Let the number of iterations t = 500, snapshots K = 5, the number of UAVs M = 1, the number of data processing points N_d =10, swarming range r =1λ, distance $d \in$ (0.1λ, 0.5λ), SNR = 0 dB. One UAV swarming system in the ideal case is used to examine the impact of unknown phase errors. Figure 43-44 show that the system still converges fast with phase errors $e_{unknown}$.

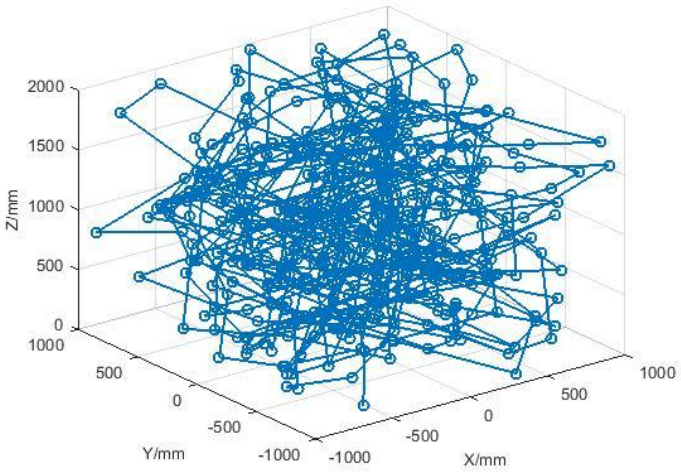

Figure 43. Diagram of one UAV swarming with number of iteration t = 500, swarming region r = 1λ, short distance $d \in (0.1\lambda, 0.5\lambda)$, and unknown phase error = $e_{unknown}$.

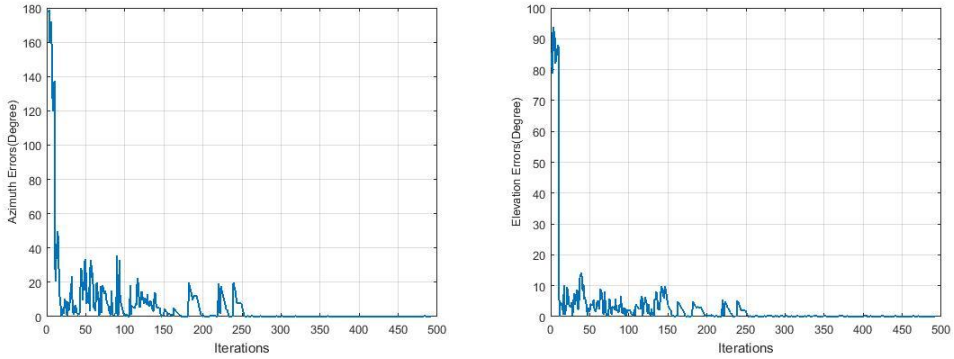

Figure 44. Simulated average of azimuth and elevation errors of ten passes with phase errors = $e_{unknown}$, and a DOA of an azimuth of 60° and elevation of 120° .

Then, take the phase errors due to UAV rotation as $e_{rotation}$, and randomly add rotation phase errors $e_{rotation}$ from -10 percent to 10 percent of 2π . The relation is:

$$e_{rotation} = 2\pi \cdot (\gamma_t \cdot 0.2 - 0.1) \tag{29}$$

where γ_t is a uniformly distributed random number between zero and one. Let the number of iterations t = 500, snapshots K = 5, the number of UAVs M = 1, the number of data processing points N_d =10, swarming range r =1λ, distance $d \in (0.1\lambda, 0.5\lambda)$, SNR = 0 dB. Figure 45-46 show that the system converges fast with phase errors $e_{rotation}$.

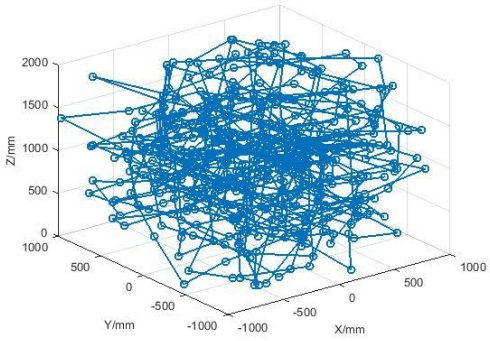

Figure 45. Diagram of one UAV swarming with number of iteration t = 500, swarming region r = 1λ, short distance $d \in (0.1\lambda, 0.5\lambda)$, phase error = $e_{rotation}$.

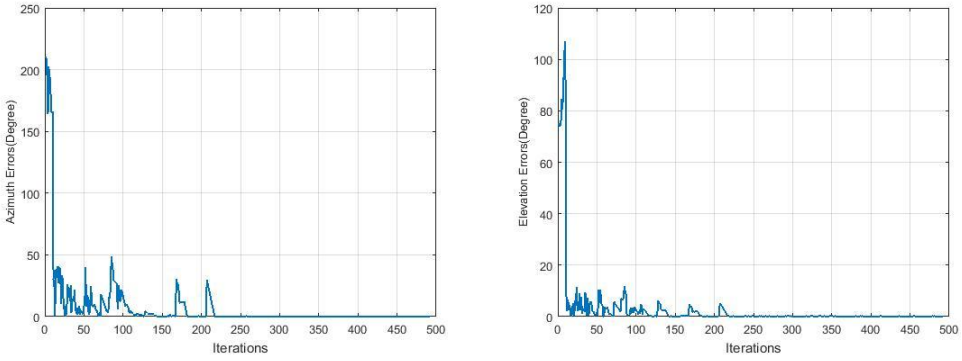

Figure 46. Simulated average of azimuth and elevation errors of ten passes with phase errors = $e_{rotation}$, and DOA of an azimuth of 60° and elevation of 120°.

Then, add both $e_{unknown}$ and $e_{rotation}$ phase errors to investigate the DOA convergence. Figure 477-48 show that the system converges fast even with both phase errors $e_{unknown}$ and $e_{rotation}$.

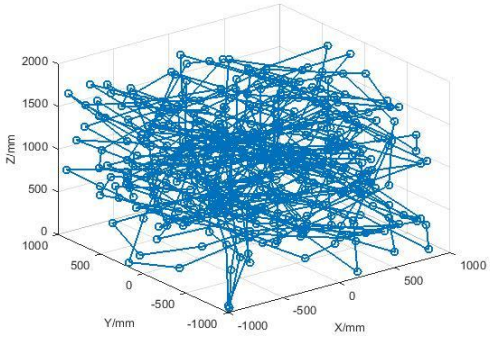

Figure 47. Diagram of one UAV swarming with number of iteration t = 500, swarming region $r = 1\lambda$, short distance $d \in (0.1\lambda, 0.5\lambda)$, phase error = $e_{unknown}$ and $e_{rotation}$.

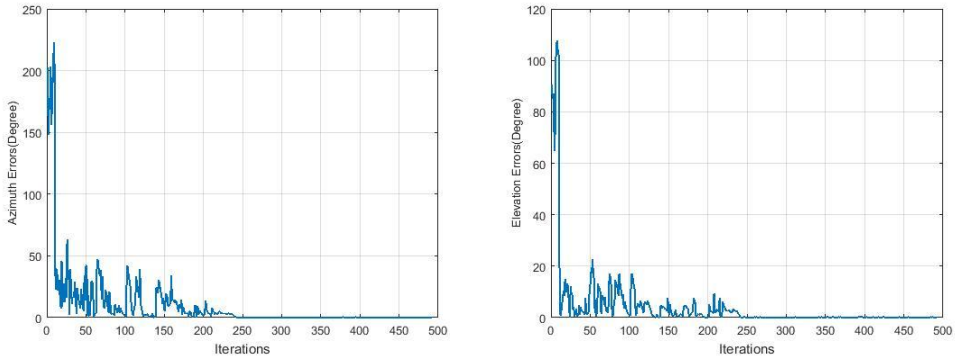

Figure 48. Simulated 10 times average of azimuth and elevation errors with phase errors = $e_{unknown}$ and $e_{rotation}$, and DOA of an azimuth of 60° and elevation of 120°.

If the unknown and rotation phase errors discussed above are satisfied with normal distribution. The probability density of normal distribution is:

$$f(x \mid \mu, \sigma^2) = \frac{1}{\sqrt{2\pi\sigma^2}} e^{-\frac{(x-\mu)^2}{2\sigma^2}} \tag{30}$$

where μ is mean or expectation of the distribution, σ is standard deviation, σ^2 is variance. The normal distribution is shown in Figure 49.

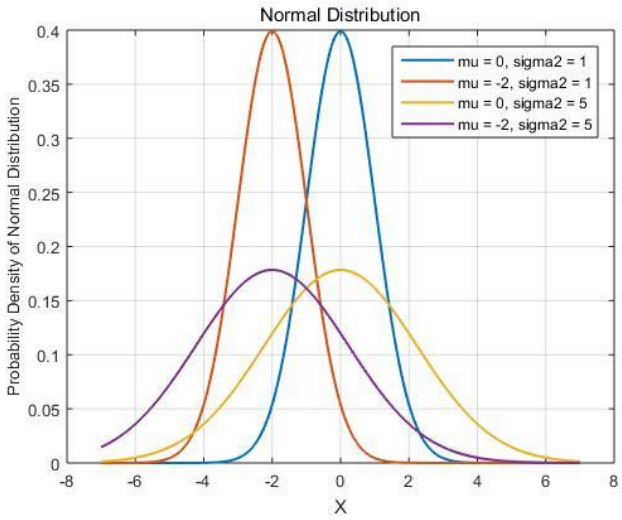

Figure 49. Normal distribution.

Take both the unknown and rotation phase errors as normal distribution phase errors. Randomly add the phase errors by varying μ and σ to investigate the impact of different type of phase error distributions.

Let the number of random number as 1000, Figure 50-53 show the 4 types of normal distribution random number created by MATLAB. The phase error relation is:

$$e_{normal\_dis} = 0.1 \cdot 2\pi \cdot normrnd(\mu, \sigma, m, n) \tag{31}$$

where m is the row and n is the column of the created error matrix.

Let the number of iterations t = 500, the number of UAVs M = 1, the number of data processing points N_d =10, SNR =0 dB, snapshots K = 5, swarming range r =1λ, distance $d \in (0.1\lambda, 0.5\lambda)$, phase error = both unknown and rotation phase errors in normal distribution. Figure 54-57 show the numerical simulation results. Figure 55 and Figure 57 tell us the system cannot converge when the normal distribution spreads out to certain range (σ = 2).

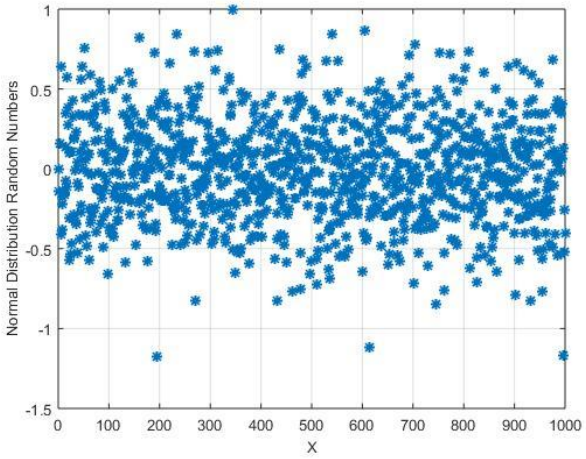

Figure 50. Normal distribution random number with μ = 0, σ = 0.5.

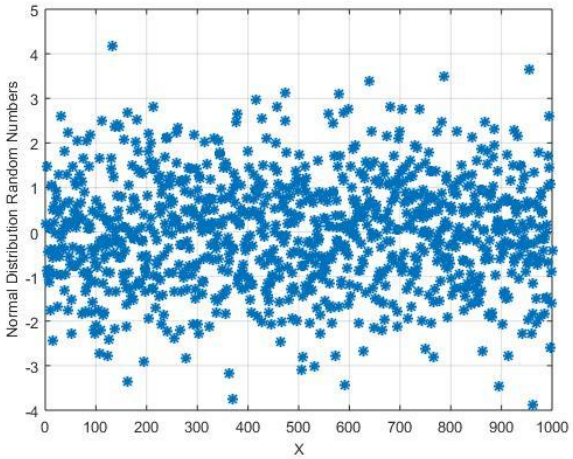

Figure 51. Normal distribution random number with μ = 0, σ = 2.

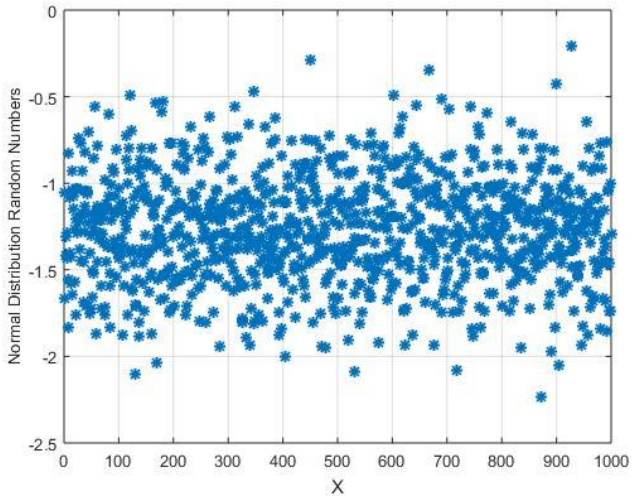

Figure 52. Normal distribution random number with μ = -2, σ = 0.5.

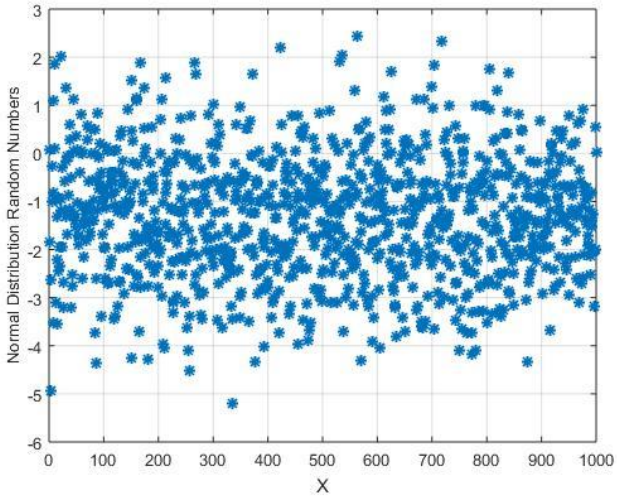

Figure 53. Normal distribution random number with μ = -2, σ = 2.

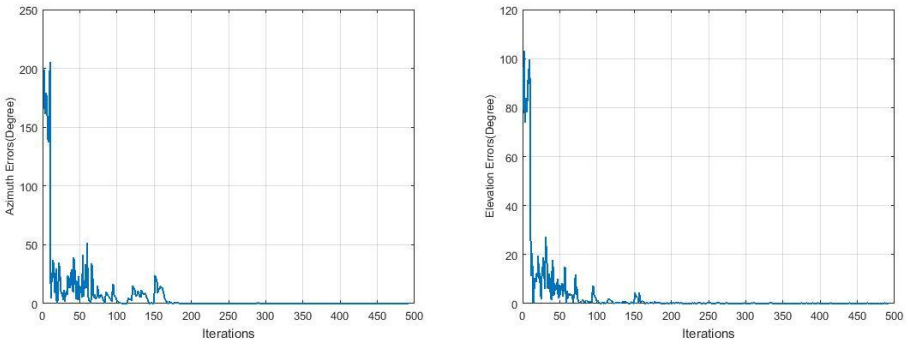

Figure 54. Simulated average of azimuth and elevation errors of ten passes with phase errors of normal distribution of $\mu = 0$, $\sigma = 0.5$, and DOA of an azimuth of 60° and elevation of 120°.

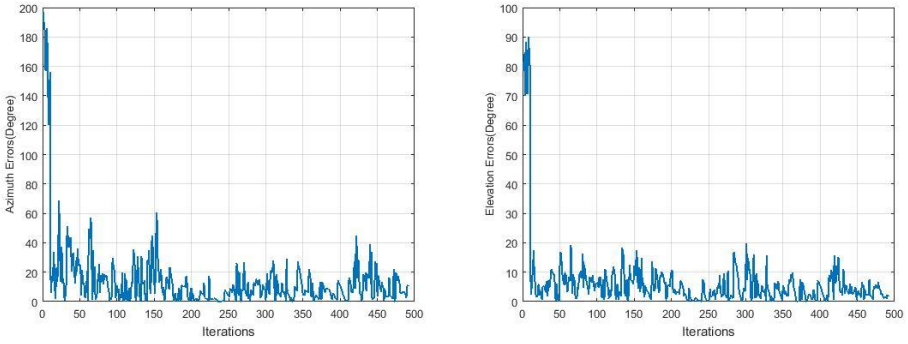

Figure 55. Simulated average of azimuth and elevation errors of ten passes with phase errors of normal distribution of $\mu = 0$, $\sigma = 2$, and DOA of an azimuth of 60° and elevation of 120°.

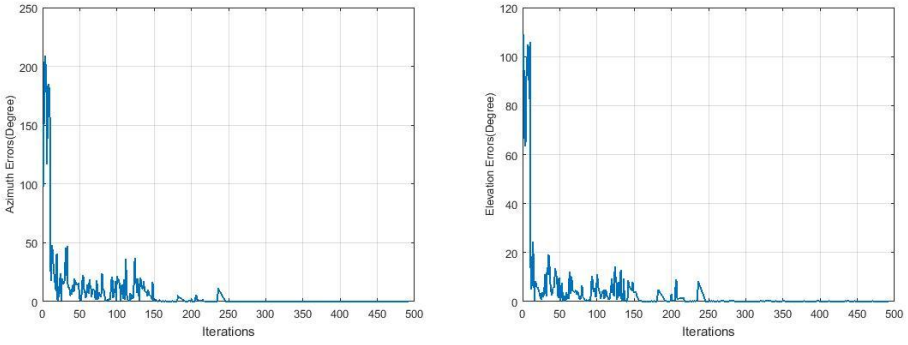

Figure 56. Simulated average of azimuth and elevation errors of ten passes with phase errors of normal distribution of $\mu = -2$, $\sigma = 0.5$, and DOA of an azimuth of 60° and elevation of 120°.

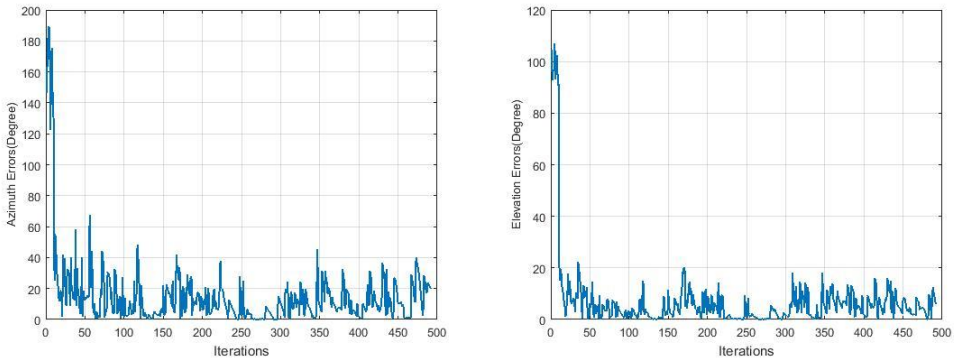

Figure 57. Simulated average of azimuth and elevation errors of ten passes with phase errors of normal distribution of μ = -2, σ = 2, and DOA of an azimuth of 60° and elevation of 120°.

3.7 Summary

In this chapter, this thesis first gives a data model for UAV swarming system and investigates the impact factors for DOA convergence based on this model in this system. A lot of impact factor are discussed in this section. The SNR, number of snapshots *K*, number of iterations *t* are directly related to the noise level. When SNR, *K* and *t* are increased, the noise will be reduced quickly. The UAV velocity is very important and should be related to wavelength, since it decides the spacing among elements in an array. The number of data points N_d is also very important because it decides the number of elements in an array. When N_d is less than 6, the system is difficult to be converged, and when the N_d is too big (e.g. great than 100), the calculation cost will be increased, so it is necessary to choose the N_d reasonably by compromising the computational complexity and DOA convergent rate. The number of UAVs *M* and swarming region *r* will not impact

the DOA convergence a lot, the convergence rate is almost the same. But when the swarming region is increased, there are more noise in the receiving data.

In the end, the impact of phase errors due to unknown noise and UAV rotation are examined in this section. Uniformly distribution and normal distribution phase errors are shown respectively. The numerical results show that the system still can converge fast, when 20 percent noise are randomly added to the ideal phase differences. However, the system will be broken up when the normal distribution is spread out to a certain range (e.g. σ =2).

4. INVESTIGATE THE DOA CONVERGENCE USING THE VOLUMETRIC RANDOM ARRAY WITH LOCATION VARYING

4.1 Introduction

Antenna array structure has a greatly impact on the DOA estimation. There are many kinds of array structures applied in the history of DOA estimation studies. However, most of research are limited to either linear (1D) or planar (2D) array. The 3D volumetric antenna array structure based on cubic and spherical configurations have been proposed having the ability to overcome aliasing and improve the accuracy of DOA estimation [4].

This work is mainly to investigate the performance of the location-varying volumetric random arrays on DOA convergence.

4.2 Location-varying Unstructured Antenna Arrays

There are thirty-two locations in the volumetric space V and sixteen elements are positioned randomly in the arbitrary sixteen locations as shown in Figure 58. The volumetric random array constructed by rectangular patch antenna randomly positioned in a 380-millimeter radius sphere to estimate the DOA.

1) At time t_1, take a measurement, calculate the DOA and store the spectrum data;

2) At time t_2, move a subset of the elements and repeat step 1;

3) At time t_3, sample and multiply MUSIC spectrum;

4) Repeat step 2 and 3 above until the DOA estimation is converged.

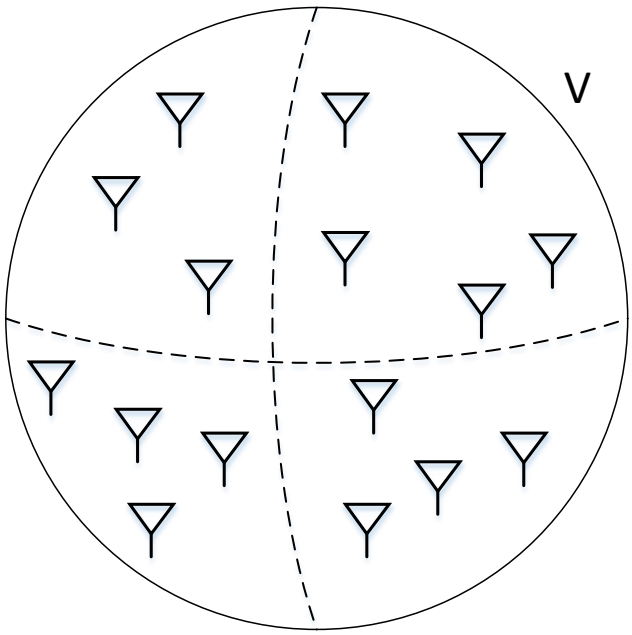

Figure 58. Schematic diagram of the receiving antenna array platform.

4.3 Simulation

Based on what we have known about the linear array, the volumetric random array configuration in this work has the capacity to accurately estimate the azimuthal angle Φ and elevation angle θ of the incident narrow band signal. The conjecture assumes that the MUSIC algorithm can estimate the DOA easily under high SNR, and increasing the numbers of iterations are helpful for the system to converge under low SNR.

Figure 59-63 show the examples of the simulated MUSIC spectrum from one to twenty iterations under different SNR conditions. Each of these has a DOA with an azimuth of 300° and elevation of 60°.

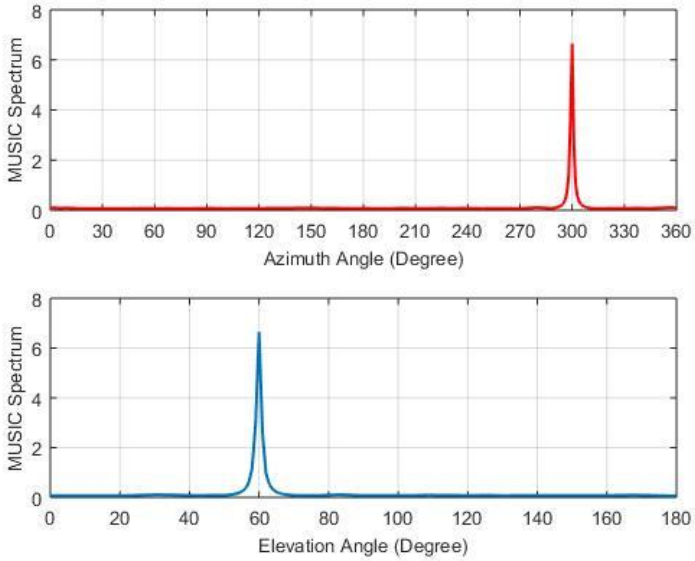

Figure 59. Simulated MUSIC spectrum with t = 1, and SNR = 0 dB.

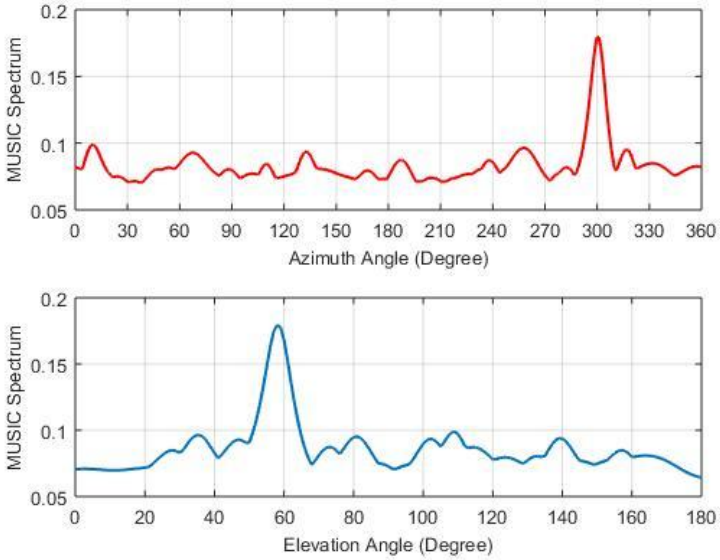

Figure 60. Simulated MUSIC spectrum with t = 1, and SNR = -10 dB.

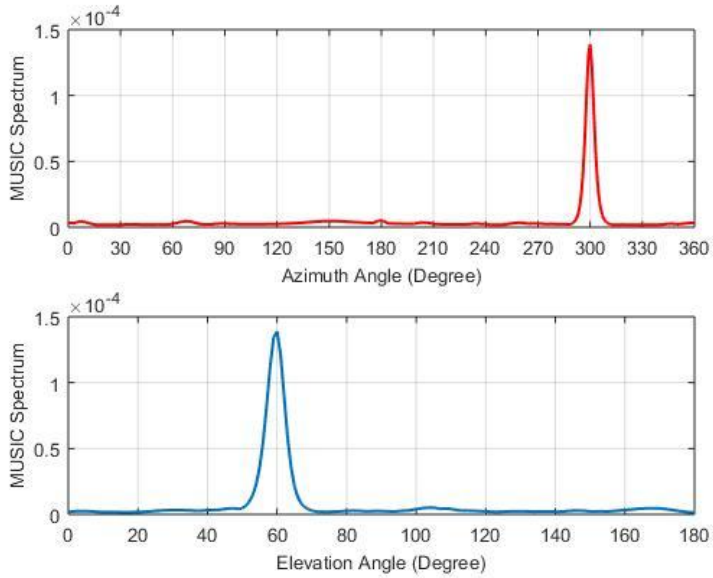

Figure 61. Simulated MUSIC spectrum with t = 5, and SNR = -10dB.

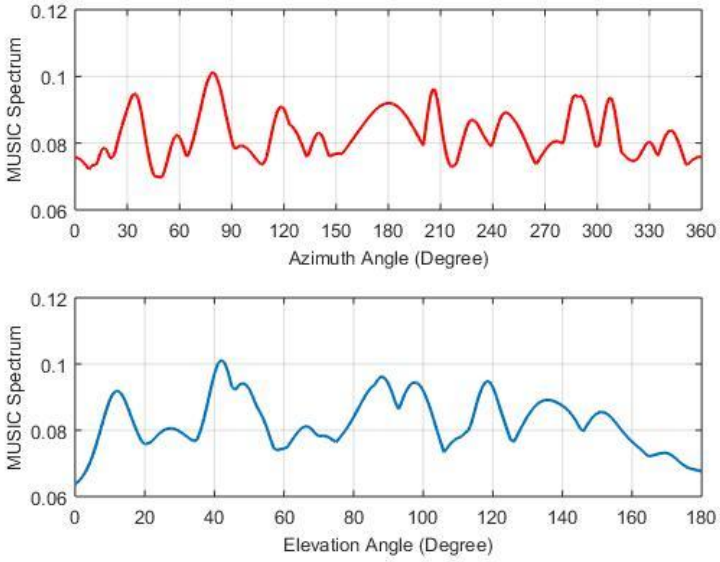

Figure 62. Simulated MUSIC spectrum with t = 1, and SNR = -15dB.

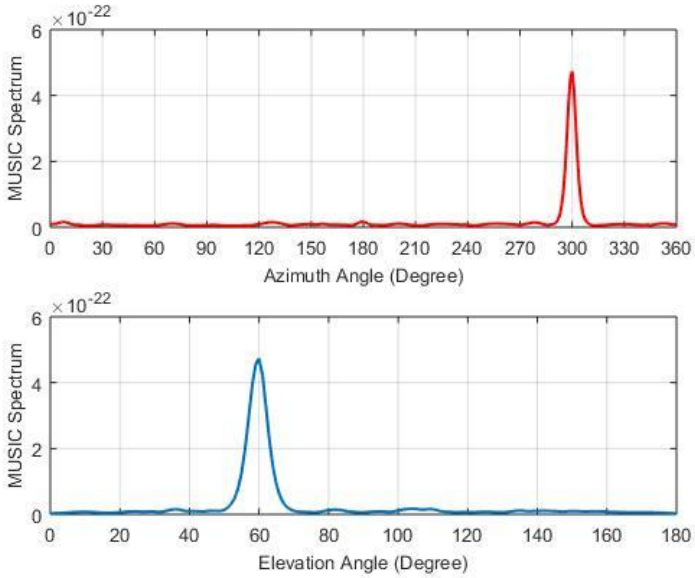

Figure 63. Simulated MUSIC spectrum with t = 20, and SNR = -15dB.

4.4 Measurement

A series of measurements at 2.45 GHz were executed to examine the convergent characteristics. A linearly polarized rectangular patch antenna positioned far enough from receiving antenna arrays to be considered in the far-field was used as a fixed source and the same sixteen rectangular patch antennas were placed randomly in the thirty-two locations as shown in the Figure 64. With the transmitting antenna connected to the port 1 and one of the receiving antennas connected to the port 2 of the vector network analyzer (VNA), the phase between the transmitting and receiving antennas was measured using S_{21}; an arbitrary special receiving antenna was chosen to calculate the phase difference.

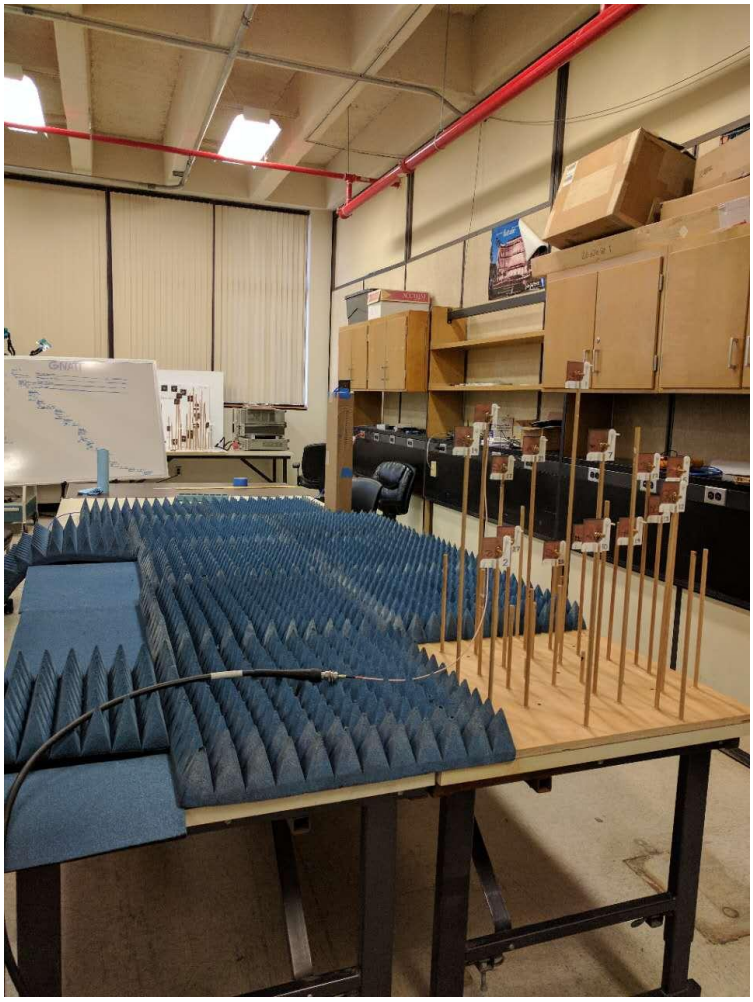

Figure 64. Test platform.

Figure 65-66 show the results obtained from one of these experiments when the transmitting antenna was placed at pre-calculated locations with the azimuthal angles 43.3° and 12.0° in two iterations. A single iteration was used to estimate the incident angles and an accurate SNR was not available. The error between theoretical expectation and practical result is within 1 to 2 degrees.

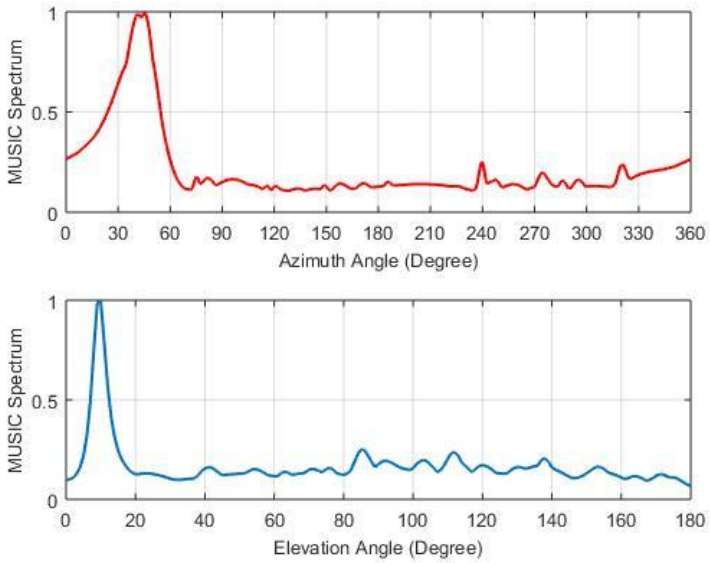

Figure 65. Measured MUSIC spectrum with t = 1, an incident signal of an azimuth of 43.3° and elevation of 12.0°.

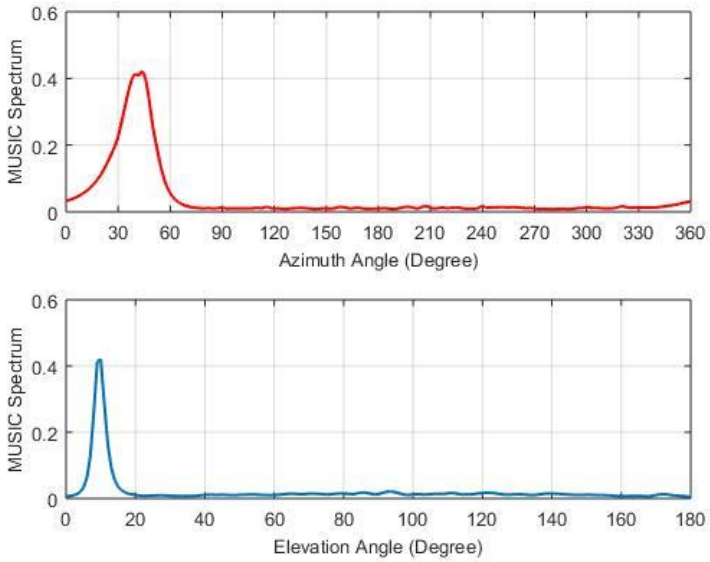

Figure 66. Measured MUSIC spectrum with t = 2, an incident signal of an azimuth of 43.3° and elevation of 12.0°.

4.5 Summary

The estimation of DOA was examined using a location-varying volumetric random array to create a synthetic receiving aperture. The simulations indicate that the technique can be utilized in very noisy environments. Experimental observations show that the system can accurately capture the azimuthal and elevation angles of the source, which also tells us the UAV swarming system is very promising in DOA estimation under very noisy conditions.

5. TUNABLE FM BAND LOCATING ANTENNA SYSTEM

5.1 Introduction

The frequency modulation (FM) broadcasting is one of the radio broadcasting and almost every city has the FM broadcasting station. This work is to detect the FM signal and investigate the performance of the low frequency electrically small antennas.

The cube is the ground plane and each face except bottom has one monopole or loop antenna. Figure 67 is the schematic diagram, there are three monopole antennas and two loop antennas, the monopole and loop antennas are opposite, since the monopole is the omnidirectional antenna. RF switch is used to control these antennas.

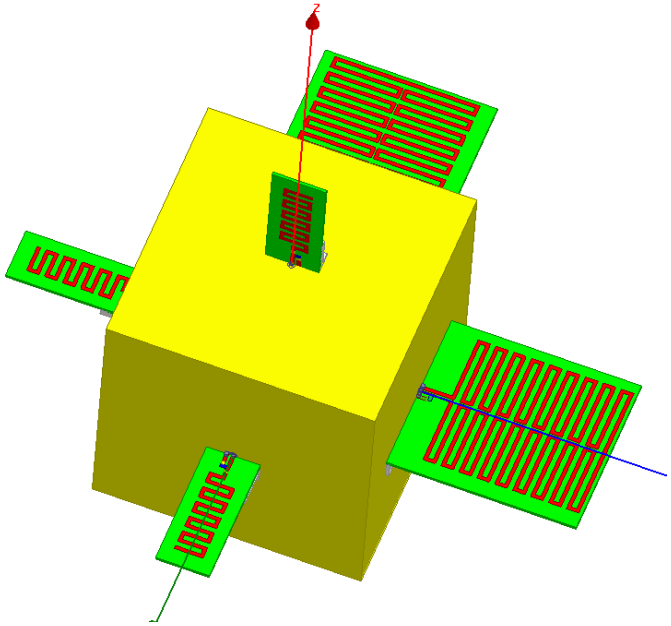

Figure 67. Simulated array diagram modeled in the HFSS.

5.2 Tunable Meandered Monopole Antenna

The wavelength for 100 MHz antenna is 3 meters, so the monopole length should be around quarter wavelength, which is 0.75 meters. The size of the monopole is too big

that meandered technology are utilized to reduce the size to less than 150 millimeters. Therefore, the monopole antenna becomes an electrically small antenna, and the gain will be very low and the bandwidth will be very small.

5.2.1 Matching Technologies for the Small Monopole Antenna

The input impedance of a short monopole is highly capacitive. Therefore, two strategies can be used as shown in Figure 68, one is series inductance and shunt inductance; the other is series inductance and shunt capacitance. Since the tunable inductance is not easy to be achieved and the capacitance can be obtained using varactor diodes, so part b is chosen to match the antenna. The capacitance C_p is mainly for matching the antenna, and the inductance L_s is mainly for tuning the antenna.

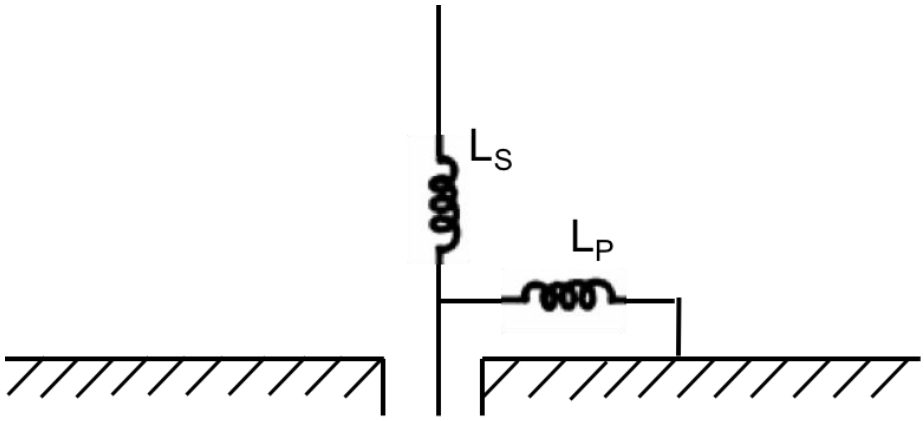

(a)

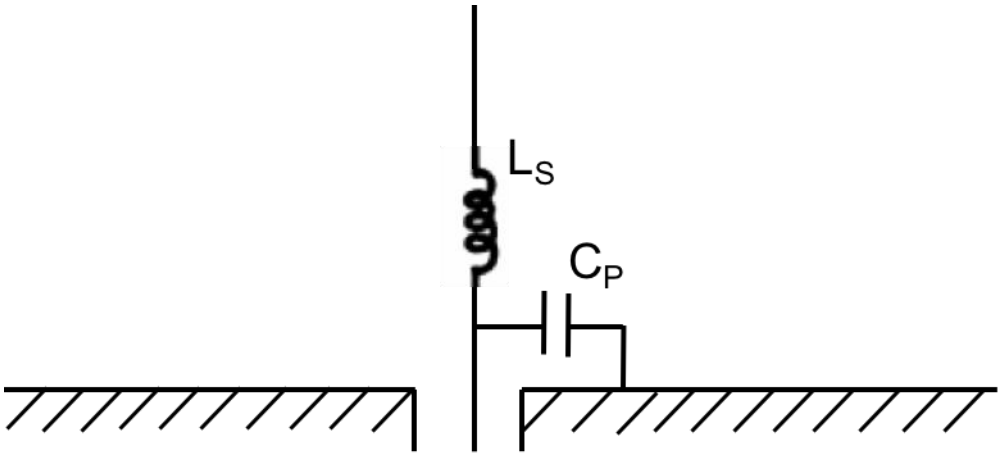

(b)

Figure 68. Matching circuit model.

5.2.2 Tuning Technology for the Small Monopole Antenna

First, use series inductance L and variable capacitance C_2 to replace the inductor L_s, and use variable capacitance C_1 to replace C_p. Here we can get:

$$j\omega L_S = j\omega L + 1/(j\omega C_2)$$

where,

$$L > L_S$$

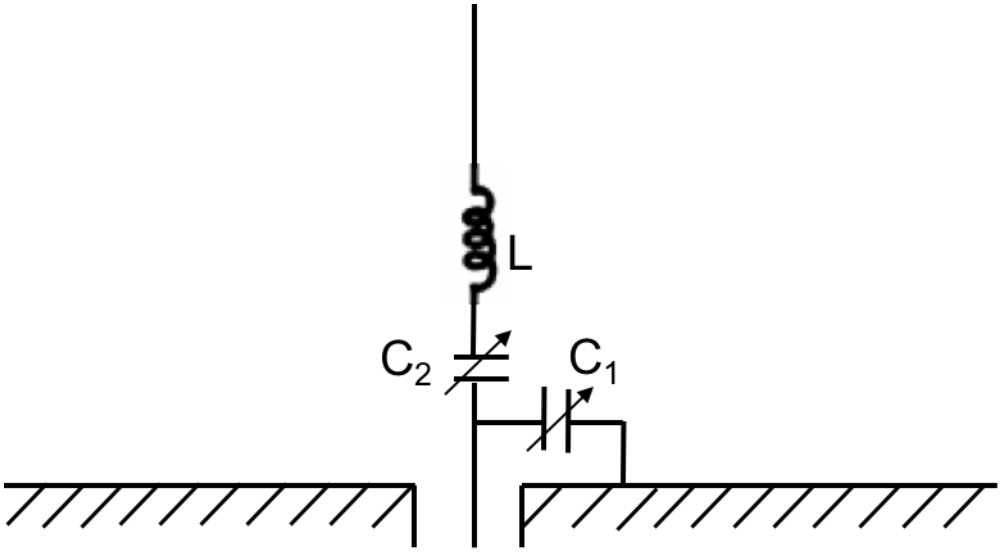

Figure 69. Tuning circuit model with variable capacitor.

However, if the antenna is required to be tuned electrically, it is necessary to use varactor diodes to replace the variable capacitance. Furthermore, voltage should be provided to control the varactor diodes. Figure 69 shows the circuit.

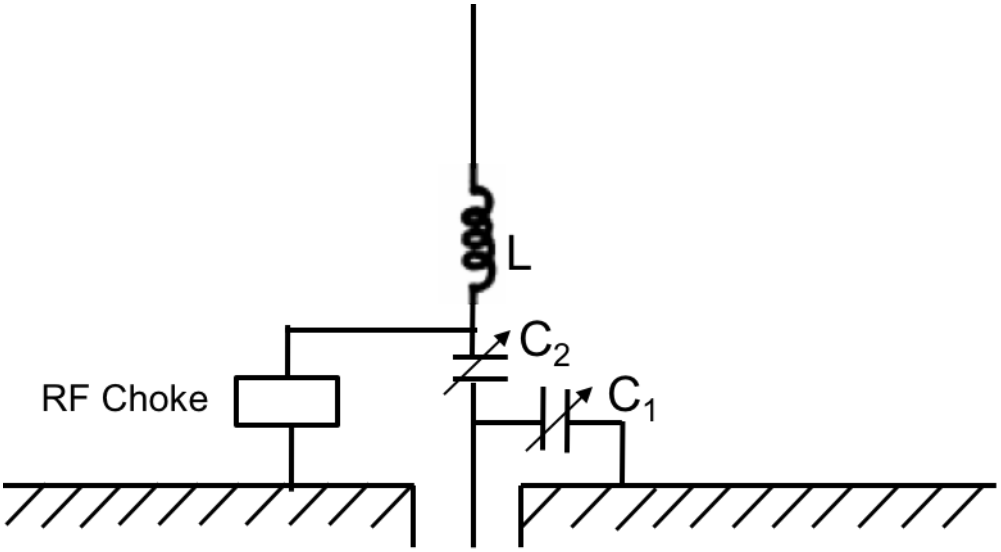

Figure 70. Tuning circuit model with varactor diode.

5.2.3 Process and Results of Simulation on HFSS

First, a metallic cube as a ground plane and a monopole with the length 150 mm are created to find the suitable value of the inductor and capacitor. The HFSS model is shown below, which matches at 101 MHz.

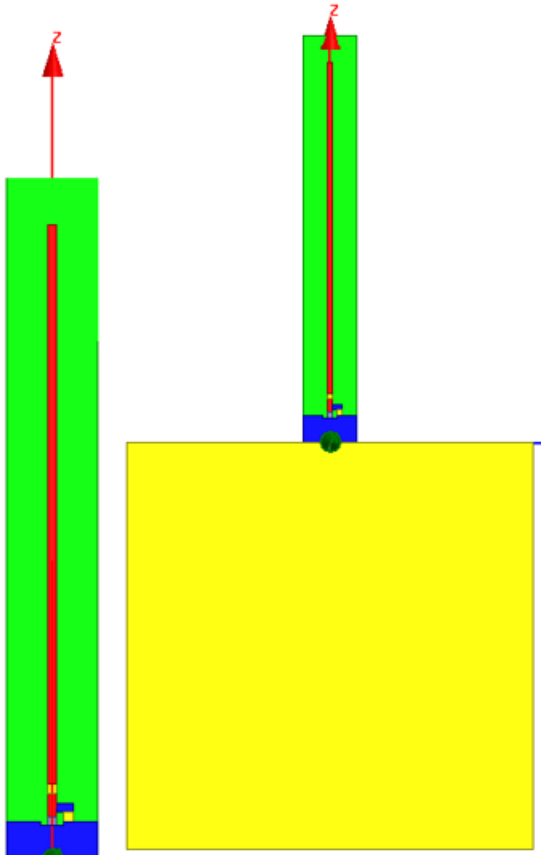

Figure 71. HFSS model for monopole antenna.

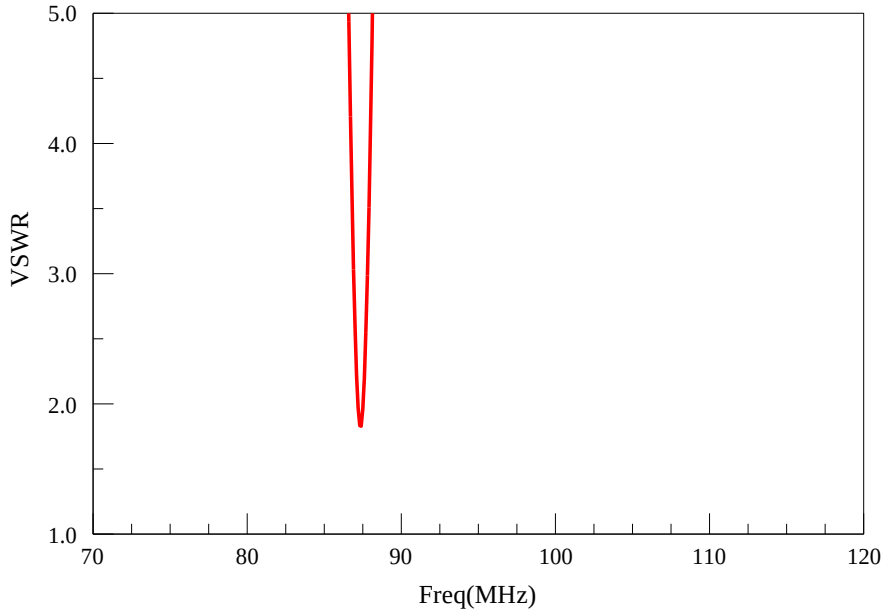

Figure 72. VSWR for monopole antenna.

Second, the size is reduced by meandering the antenna and tuning inductor and capacitor slightly. The model is shown below, and the S_{11} simulation results show that the antenna can be tuned in the FM band. Moreover, the simulation results demonstrate that the series inductor is mainly for tuning and the shunt capacitor is mainly for matching. Also, the gain of the antenna is very low.

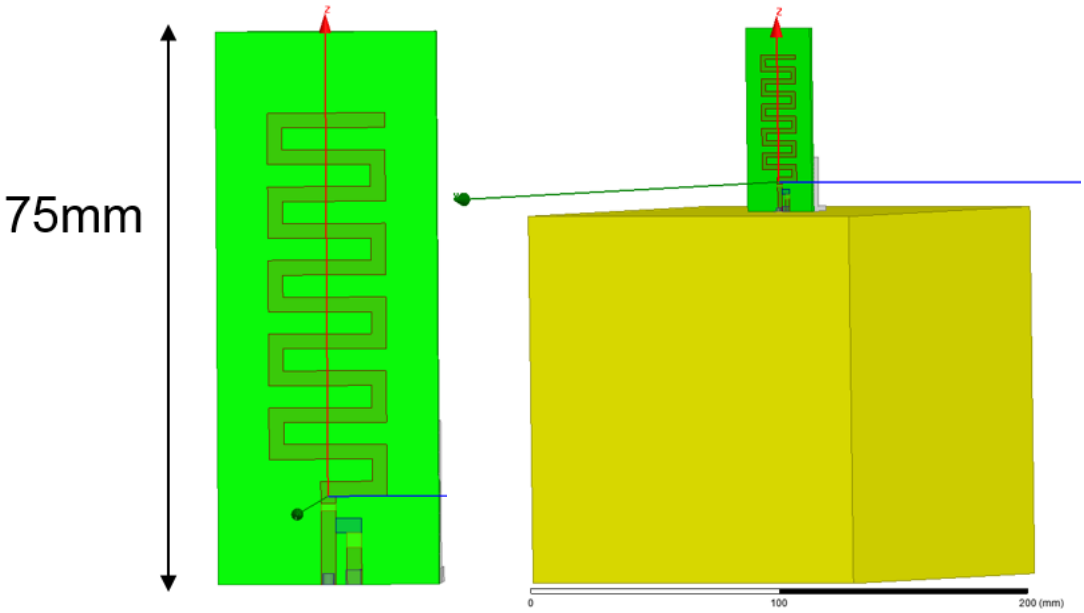

Figure 73. HFSS model for meandering monopole antenna.

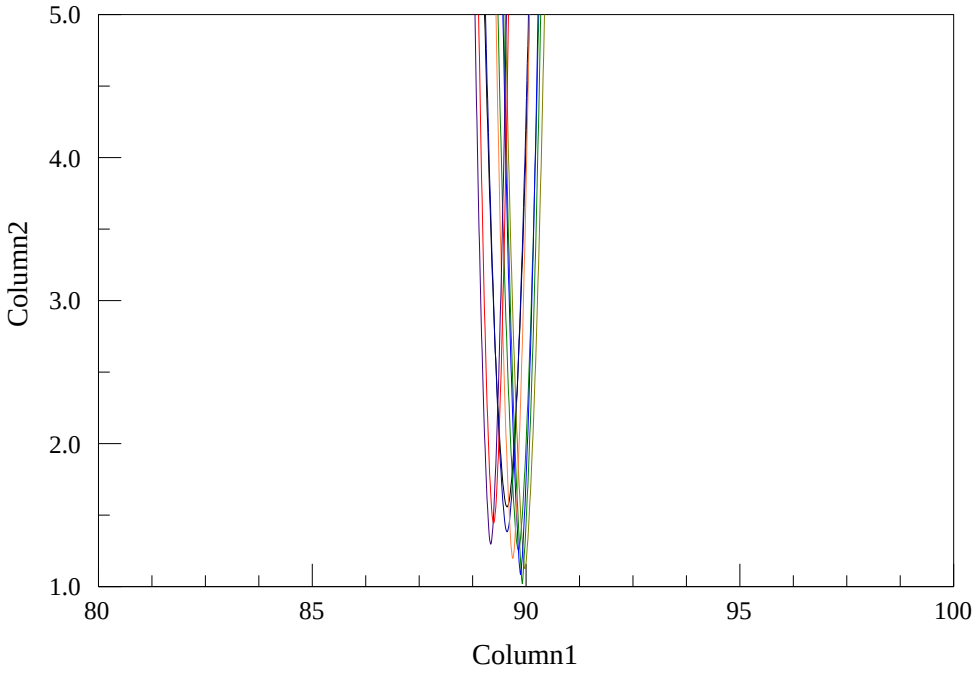

Figure 74. VSWR as the shunt capacitor varies.

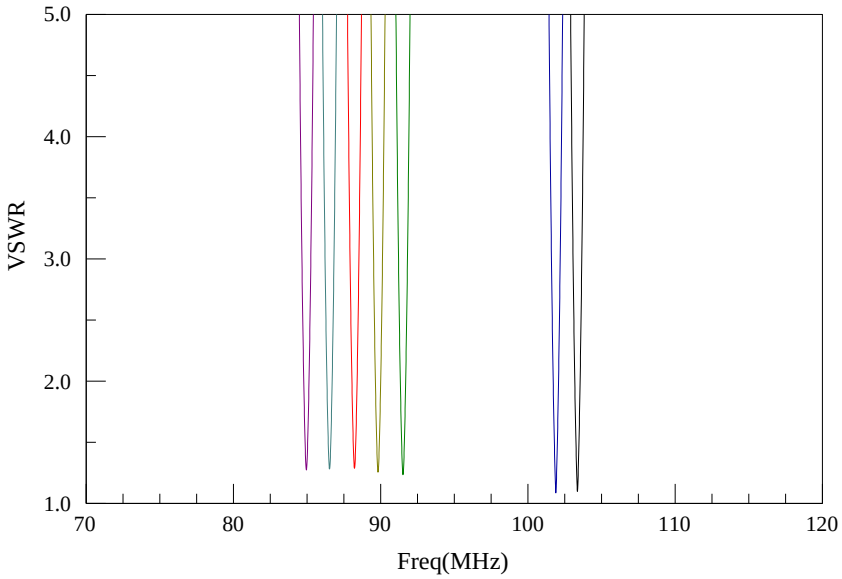

Figure 75. VSWR as the series inductor varies.

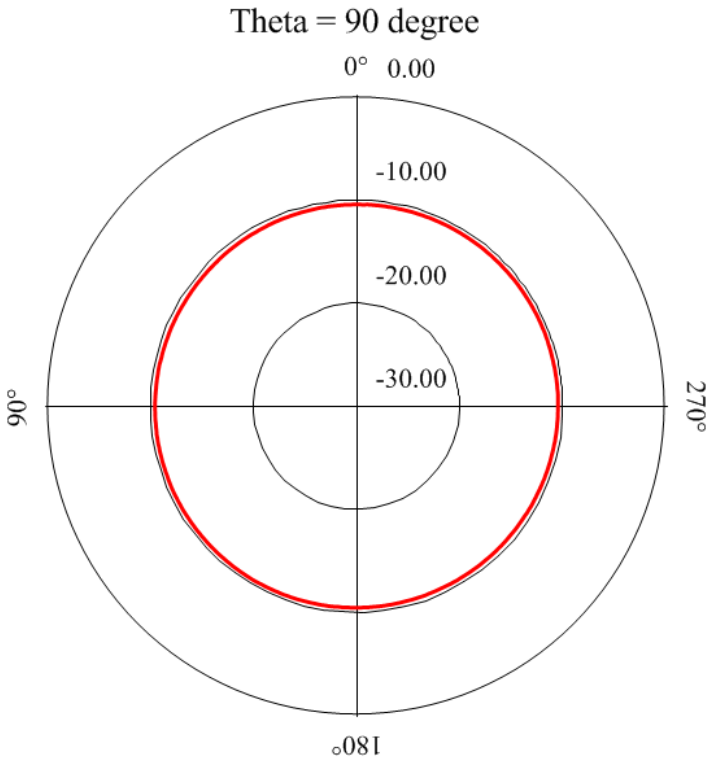

Figure 76. Simulated radiation pattern.

At last, varactor diodes are used to replace the capacitor and ass RF choke using shunt inductor to provide the power for varactor diode. The HFSS model and simulation data is shown below.

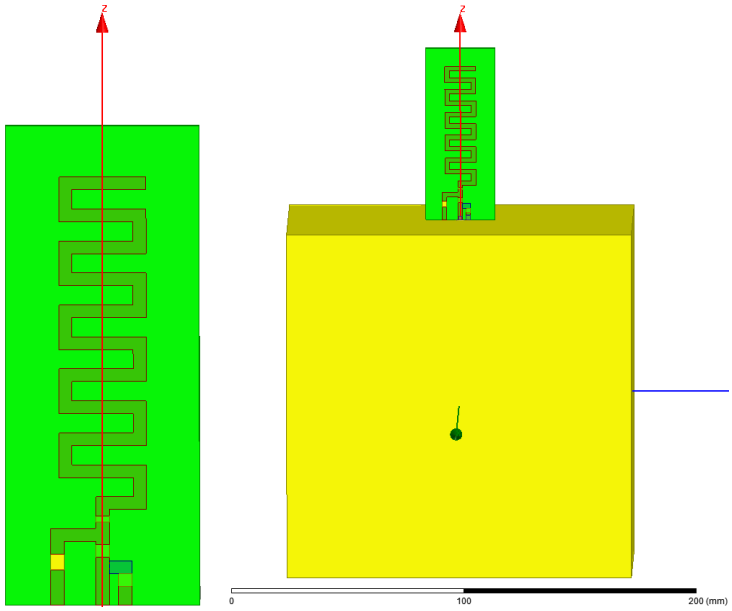

Figure 77. HFSS model for adding varactor diode and RF choke.

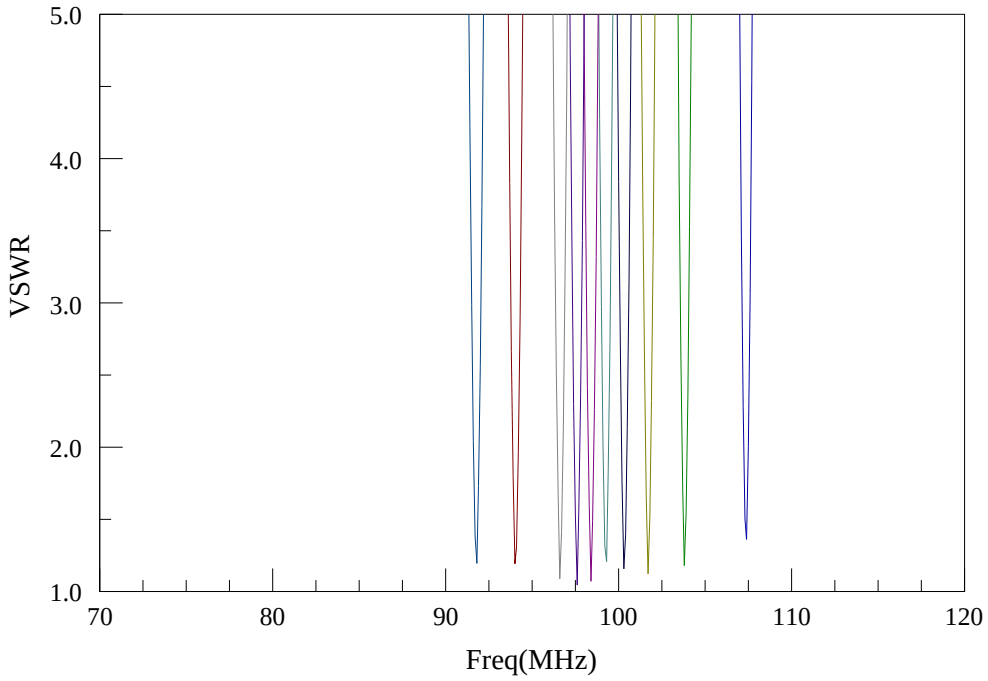

Figure 78. Simulated VSWR for tunable monopole antenna.

5.2.4 Measurement

The fabricated loop antenna is shown below. The substrate of the antenna is FR-4 and its dielectric constant is 4.1.

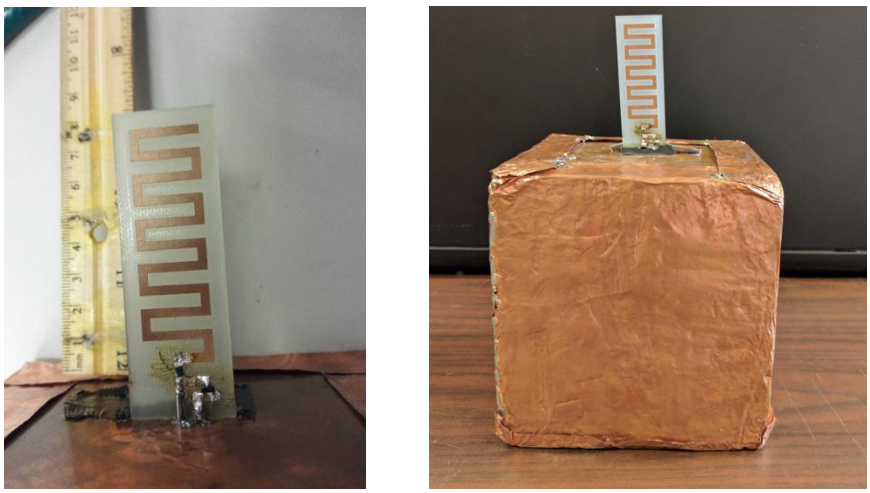

Figure 79. Fabricated monopole antenna.

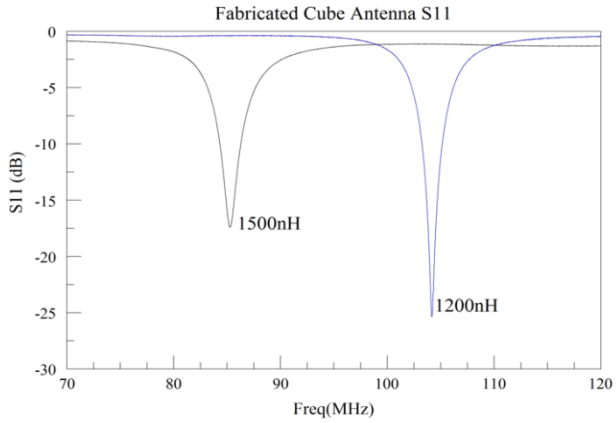

Figure 80. S_{11} of the fabricated monopole antenna.

5.3 Loop Antenna

The analysis of the loop antenna is same as the monopole antenna, so the process will be simplified.

5.3.1 Matching Technologies for the Small Loop Antenna

The input impedance of a short loop antenna is highly inductive impedance. So, two strategies can be used as shown in Figure 81, one is series capacitance and shunt capacitance; the other is series capacitance and shunt inductance. Since the tunable inductance is not easy to be achieved and the tunable capacitance can be obtained using varactor diodes, part b is chosen in Figure 81 to match the antenna. The capacitance C_p and inductance L_p is mainly for matching the antenna, and the capacitance C_s is mainly for tuning the antenna.

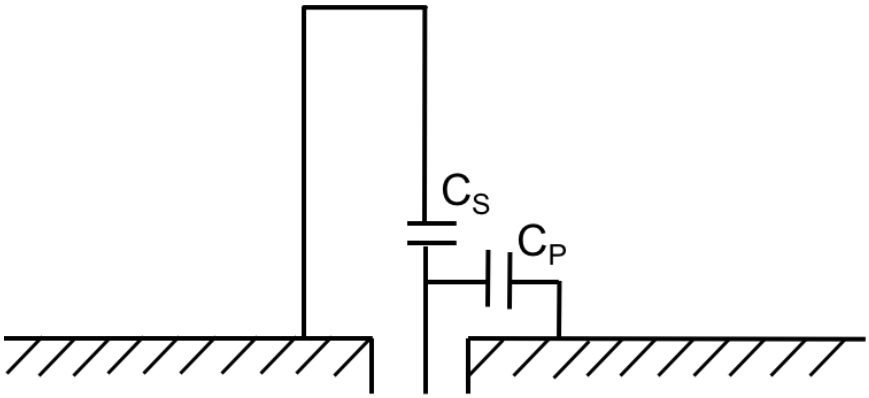

(a)

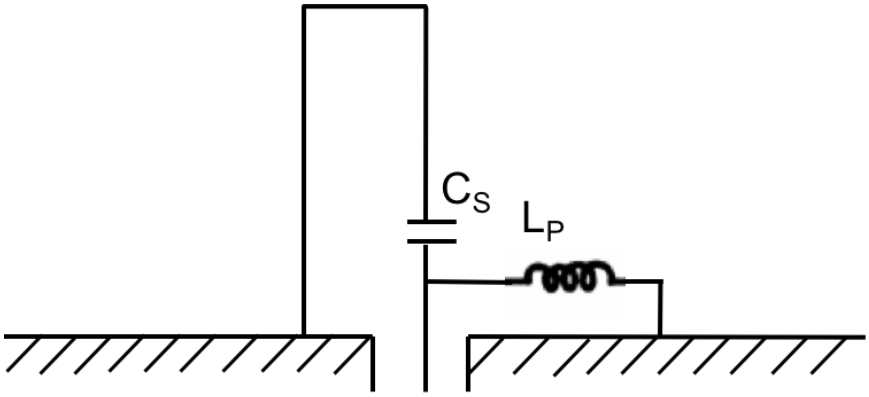

(b)

Figure 81. Matching circuit model for loop antenna.

5.3.2 Tuning Technology for the Small Loop Antenna

Different from the technology of tuning monopole antenna, the loop antenna can be directly tuned with the series capacitance, then the varactor diode is used to replace the capacitor. The model is shown below.

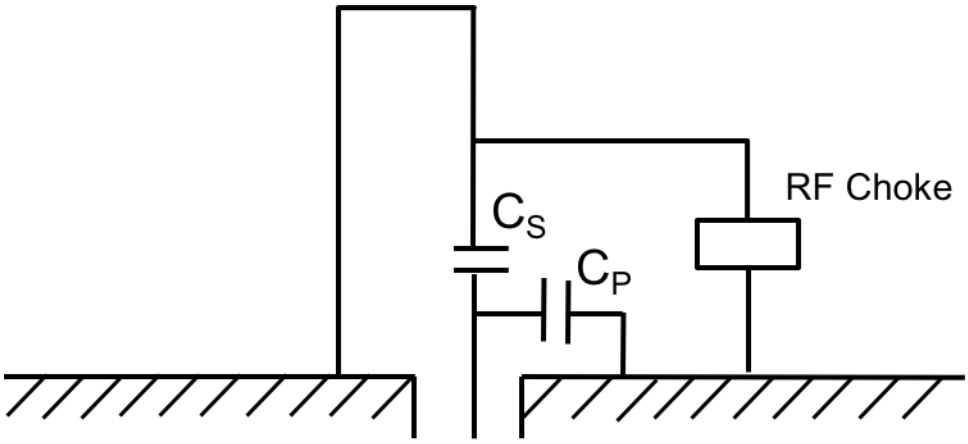

Figure 82. Tuning circuit model with varactor diode Cs.

5.3.3 Process and Data of Simulation on HFSS

The process is the same as the process of the monopole antenna design. First, a metallic cube as a ground plane and a loop antenna with the length 400 mm are created to find the suitable value of the inductor and capacitor. The HFSS model is shown below, which matches at 88 MHz.

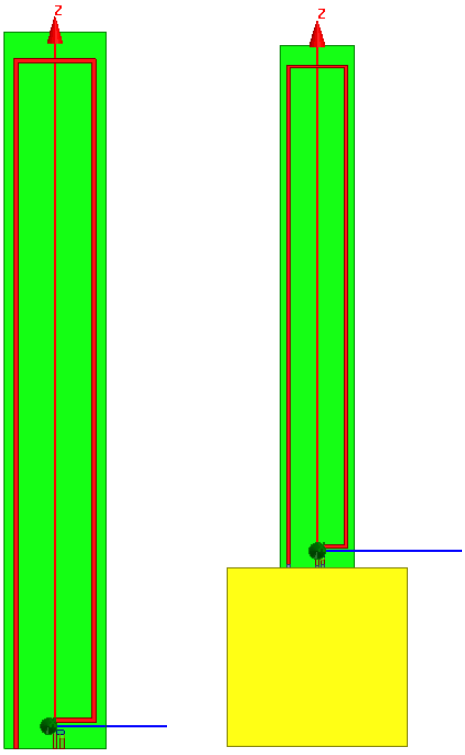

Figure 83. HFSS model for loop antenna.

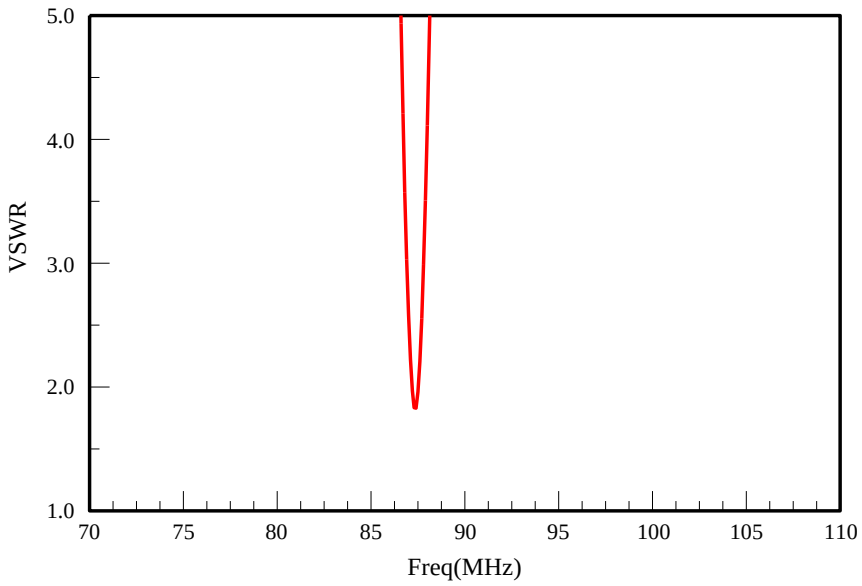

Figure 84. VSWR for loop antenna.

Second, the size is reduced by meandering the antenna and tuning the capacitors slightly. The model is shown below, and the VSWR simulation results show that the antenna can be tuned in the FM band. But the tuning range is smaller than the tuning range of tunable monopole antenna above. Also, the gain of the antenna is very low.

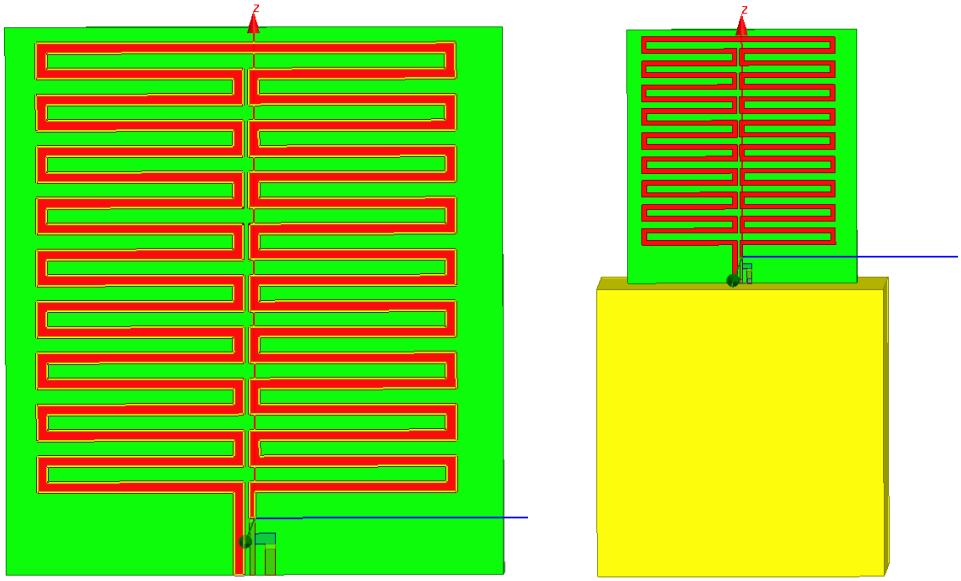

Figure 85. HFSS model for meandering loop antenna.

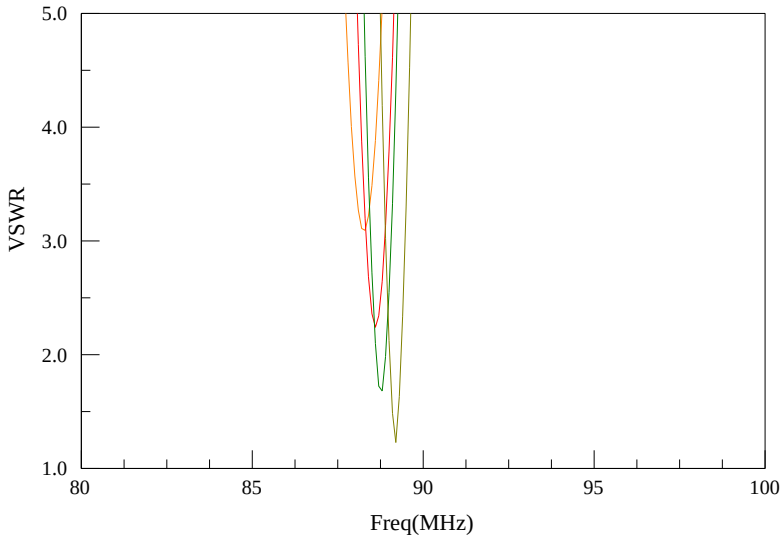

Figure 86. VSWR as the shunt capacitor varies.

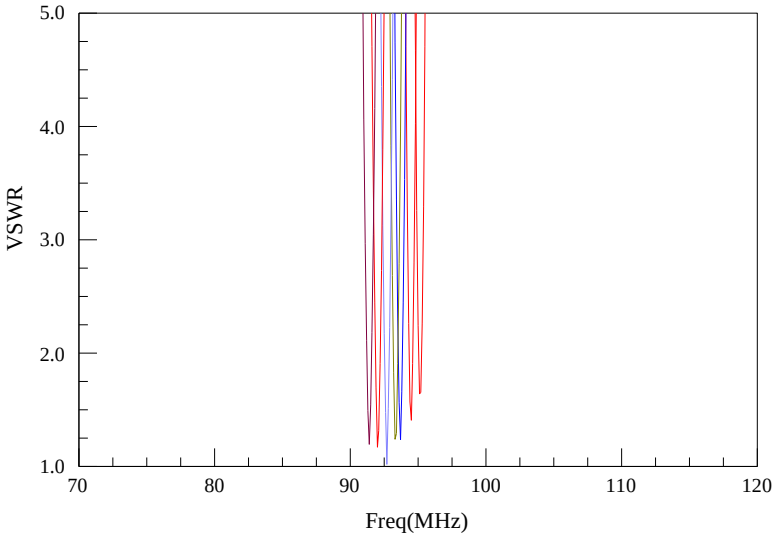

Figure 87. VSWR as the series capacitor varies.

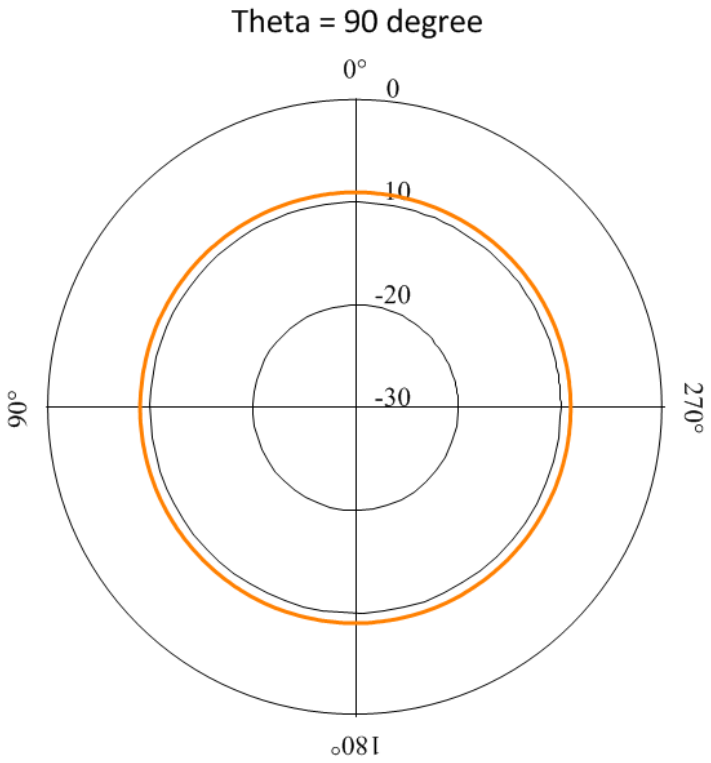

Figure 88. Radiation pattern for meandering loop antenna.

At last, varactor diodes are used to replace the series capacitor and add RF choke using shunt inductor to provide the power for varactor diode. The HFSS model and simulation data is shown below.

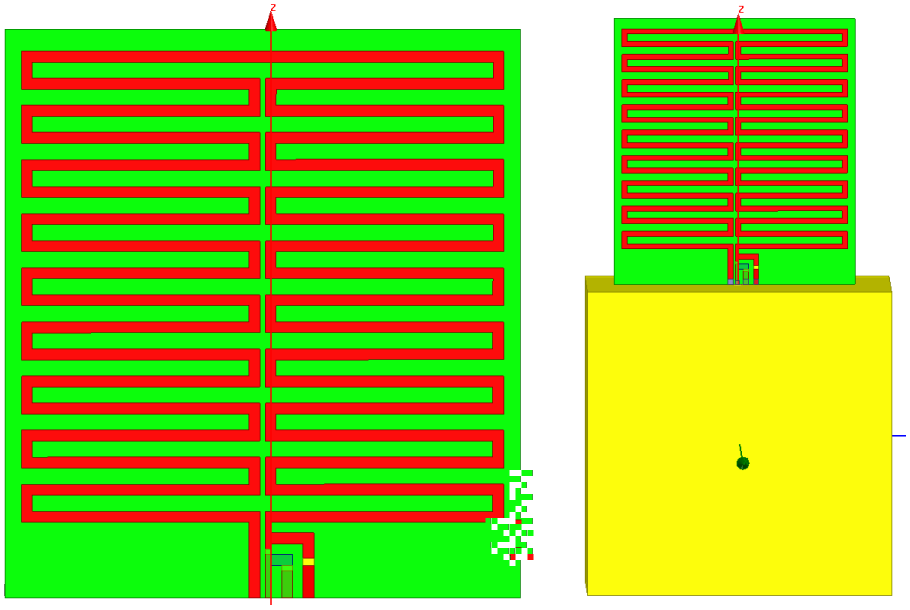

Figure 89. HFSS model with varactor diode and RF choke.

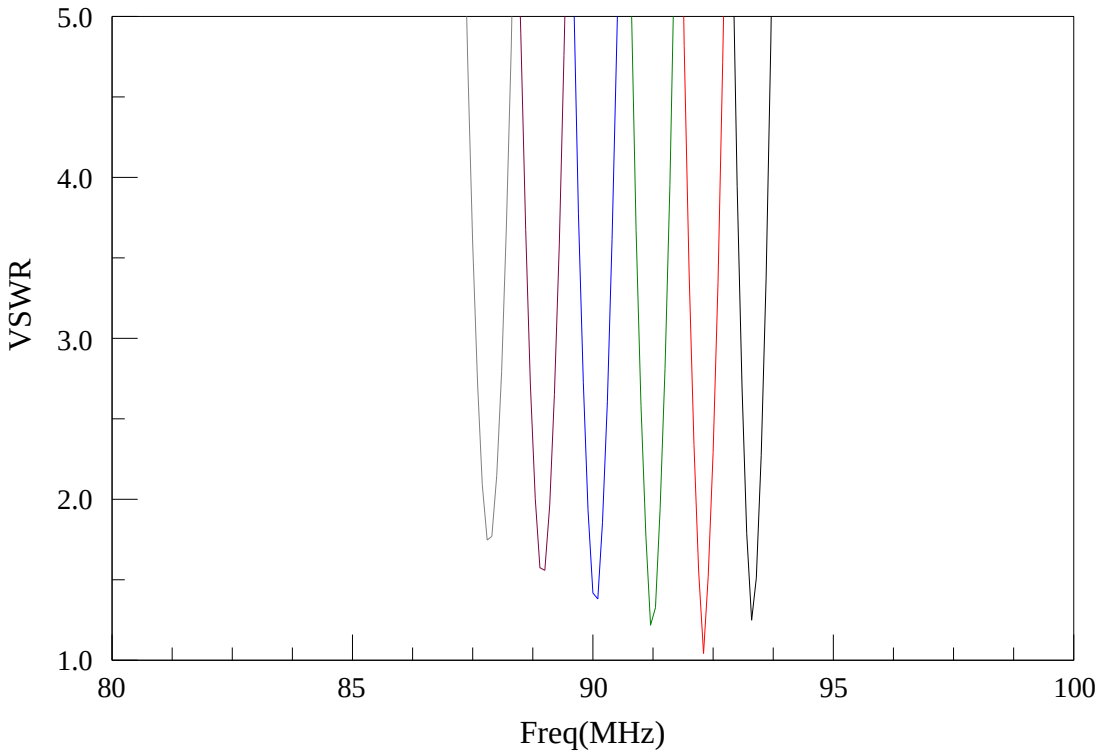

Figure 90. Simulated VSWR for tunable loop antenna.

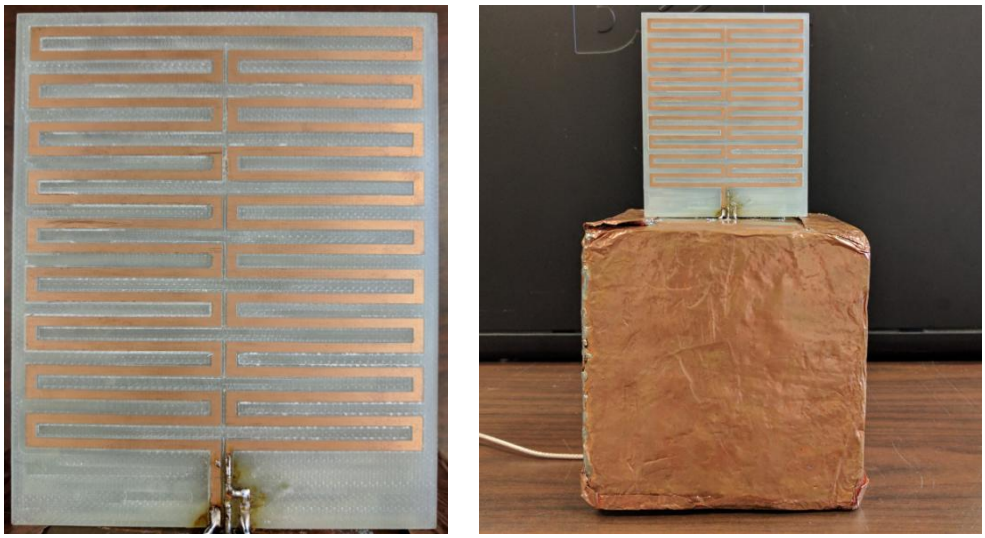

Figure 91. Fabricated loop antenna.

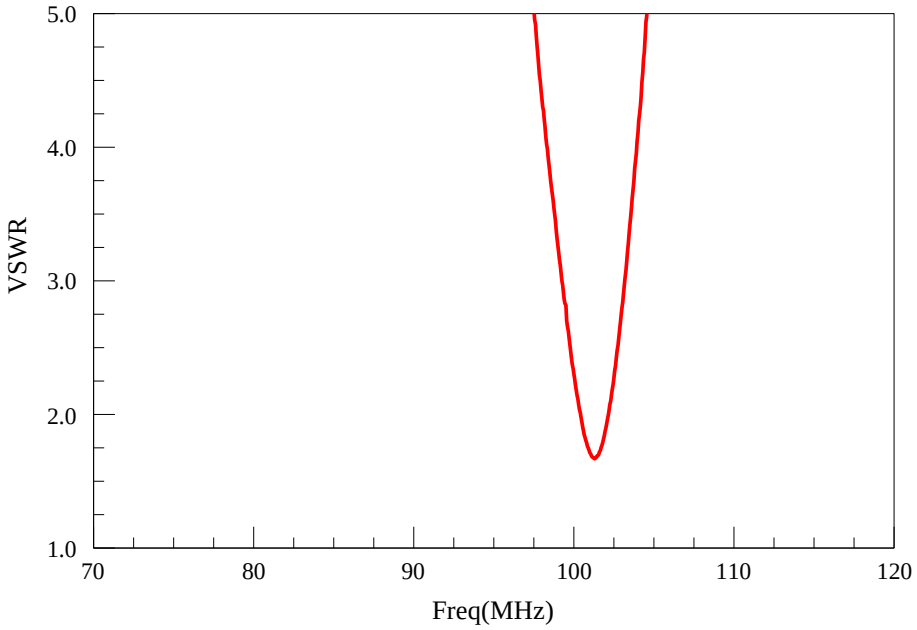

Figure 92. VSWR of the fabricated monopole antenna.

5.4 Discussion and Summary

The electrically small monopole and loop antenna can be tuned electrically, however, the gain is so low that the local FM signal cannot be detected. Since the antenna gain is low, the SNR becomes very small. The amplifier should be added to the antenna, if we still want to use the system to detect the FM signals.

6. CONCLUSION

6.1 Conclusions

The thesis first examines the ramifications of using unstructured arrays for 2D DOA estimation based on sub-space techniques. This work successfully applies the FD domain Root-MUSIC onto 2D DOA estimation in volumetric random arrays.

Second, this thesis comes up with a data model for the UAV swarming system. Based on this model, this thesis investigates the impact factors for DOA estimation in the UAV swarming system. Furthermore, this thesis discusses the impact of phase errors for DOA convergence. It shows that the swarming system offers a high performance of DOA convergence.

Third, the location-varying simulation and experiment show that the space-varying with time method can be used in a very noisy condition. Moreover, it shows that the UAV swarming system can be applied into a very noisy condition and has a good promising.

REFERENCES

[1] R. O. Schmidt, “Multiple emitter location and signal parameter estimation,” IEEE Trans. on AP., Vol. 34, pp. 276-280, 1986.

[2] C. R. Dongarsane and A. N. Jadhav, “Simulation study on DOA estimation using MUSIC algorithm,” Intl. J. Tech. Eng. Sys., vol. 2(1), Mar. 2011.

[3] H. Tang, “DOA estimation based on MUSIC algorithm,” Master thesis, Kalmar, May 2015.

[4] Z. Xia, G. H. Huff, J.-F. Chamberland, H. Pfister, R. Bhattacharya, “Direction of arrival estimation using canonical and crystallographic volumetric element configurations,” in 6th EUCAP, Prague, 26-30, pp. 1436-1439, Mar. 2012.

[5] P. Stcica, “Maximum likelihood method for direction of arrival estimation,” IEEE Trans. on ASSP. Vol.38(7). pp. 1132~1143, 1990.

[6] M. L. Miller, “Maximum likelihood narrow-band direction finding and EM algorithms,” IEEE Trans. on ASSP. Vol.36(10). pp.1560~1577, 1990.

[7] I. Ziskind, and M. Wax, “Maximum likelihood localization of multiple sources by alternating projection,” IEEE Trans. on ASSP. Vol.36(10). pp. 1553~1560, 1998.

[8] R. D. Degrot, “The contained MUSIC problem,” IEEE Trans. on SP. Vol.41(3). pp. 1445~1449, 1993.

[9] F. Richard, “Analysis of min-norm and MUSIC with arbitrary array geometry,” IEEE Trans. on AES. Vol.26(6). pp. 976~985, 1990.

[10] M. Rubsamen, and A. B. Gershman. “Direction-of-arrival estimation for nonuniform sensor arrays: from manifold separation to Fourier domain MUSIC methods,” IEEE Trans. on SP. Vol.57(2). pp. 588~599, 2009.

[11] P. Stonica, etc., “MUSIC maximum likelihood and Cramer-Rao bound,” IEEE Trans. on ASSP. Vol.37(5). pp.720~741, 1989.

[12] H. B. Lee, etc., “Resolution threshold beamspace MUSIC for two closely spaced emitters,” IEEE Trans. on ASSP. Vol.38(9). pp. 723~738, 1990.

[13] A. J. Barabell, “Improving the resolution performance of eigenstructure-based direction-finding algorithms,” in Proc. ICASSP. pp. 336~339, 1983.

[14] B. D. Rao, and K. V. Hari, “Performance of analysis of root-MUSIC,” in IEEE Trans. on ASSP. Vol.37(12). pp. 1939~1949, 1989.

[15] M. Gavish, etc., “Performance analysis of the VIA ESPRIT algorithm,” IEE-Proc-F. Vol.140(2). pp. 123~128, 1993.

[16] S. V. Schell, R. A. Calabretta, W. A. Gardner, and B. G. Agee, “Cyclic MUSIC algorithm for signal-selective direction estimation,” in Proc. ICASSP’ 89 Conf. pp. 2278~2281, 1989.

[17] R. Roy and T. Kailath, "ESPRIT-Estimation of signal parameters via rotational invariance techniques," in IEEE Trans. on ASSP. Vol. 37(7), pp. 984-995, 1989.

[18] B. Friedlander, and A. J. Weiss, “Direction finding for wide-band signals using an interpolated array,” in IEEE Trans. on SP. Vol. 41(4), pp. 1618-1634, 1993.

[19] B. Friedlander, and A. J. Weiss, “Direction finding using spatial smoothing with interpolated arrays,” in IEEE Trans. on Aerosp. Electron. Syst. Vol. 28(4), pp. 574-587, 1992.

[20] M. A. Doron, and E. Doron., “Wavefield modeling and array processing, part I—spatial sampling,” in IEEE Trans. on SP. Vol. 42, pp. 2549-2559, 1994a.

[21] M. A. Doron, and E. Doron., “Wavefield modeling and array processing, part II—Algorithm,” in IEEE Trans. on SP. Vol. 42, pp. 2560-2570, 1994b.

[22] M. A. Doron, and E. Doron., “Wavefield modeling and array processing, part III—Resolution Capacity,” in IEEE Trans. on SP. Vol. 42, pp. 2571-25800, 1994c.

[23] B. Friedlander, and A. J. Weiss, “Direction finding in the presence of mutual coupling,” in IEEE Trans. on AP. Vol. 39(3), pp. 273-284, 2002.

[24] Z. Chen, J.-F. Chamberland, G. H. Huff, “Impact of UAV swarm density and heterogeneity on synthetic aperture DOA convergence,” in IEEE AP-S symposium on antenna and propagation and USNC-URSI radio science meeting, July 2017.